Dissipation and quantum phase transitions of a pair of Josephson junctions

Dissipation and quantum phase transitions of a pair of Josephson junctions

Gil Refael,[1] Eugene Demler,[1] Yuval Oreg,[2] and Daniel S. Fisher[1]
[1]*Department of Physics, Harvard University, Cambridge, Massachusetts 02138, USA*
[2]*Department of Condensed Matter Physics, Weizmann Institute of Science, Rehovot, 76100, Israel*
(Received 2 March 2003; revised manuscript received 7 October 2003; published 24 December 2003)

A model system consisting of a mesoscopic superconducting grain coupled by Josephson junctions to two macroscopic superconducting electrodes is studied. We focus on the effects of Ohmic dissipation caused by resistive shunts and superconducting-normal charge relaxation within the grain. As the temperature is lowered, the behavior crosses over from uncoupled Josephson junctions, similar to situations analyzed previously, to strongly interacting junctions. The crossover temperature is related to the energy-level spacing of the grain and is of the order of the inverse escape time from the grain. In the limit of zero temperature, the two-junction system exhibits five distinct quantum phases, including a novel superconducting state with localized Cooper pairs on the grain but phase coherence between the leads due to Cooper pair cotunneling processes. In contrast to a single junction, the transition from the fully superconducting to fully normal phases is found to be controlled by an intermediate-coupling fixed point whose critical exponents vary continuously as the resistances are changed. The model is analyzed via two-component sine-Gordon models and related Coulomb gases that provide effective low-temperature descriptions in both the weak and strong Josephson coupling limits. The complicated phase diagram is consistent with symmetries of the two component sine-Gordon models, which include weak- to strong-coupling duality and permutation triality. Experimental consequences of the results and potential implications for superconductor to normal transitions in thin wires and films are discussed briefly.

DOI: 10.1103/PhysRevB.68.214515 PACS number(s): 74.81.Fa, 74.78.Na

I. INTRODUCTION

Understanding the effects of dissipation on quantum phase transitions has proved to be a challenging problem in many contexts including quantum Hall transitions[1] and quantum critical points in antiferromagnets.[2] Transitions from superconductor to ''normal'' metal or insulator in thin wires and films have been extensively studied,[3–10] as well as in Josephson junction arrays[11–19] and superconducting nanowires.[20–27] One of the most intriguing aspects of these transitions is the role of dissipation.[28–33] Theoretically, there has been extensive work on the effects of dissipation on a single resistively shunted Josephson junction (RSJJ). The resistor can be modeled theoretically as a Caldeira-Leggett Ohmic heat bath,[34–42] and precise predictions for the transport properties can be worked out (see Ref. 43 for a review). The system undergoes a superconductor-to-normal transition at zero temperature when the shunt resistance increases through a critical value equal to the quantum of resistance $R_Q = h/4e^2 = 6.53\ \mathrm{k}\Omega$. Recent experiments by Penttilä *et al.*[44] showed good agreement with the theoretical analysis.

Arrays of RSJJ's have been studied in the same framework in terms of the *local* physics of the individual junctions.[43,45–52] By percolation arguments, this local physics has been argued to apply to granular films and wires with the superconductor-to-normal transition in these extended systems occurring when the *individual* shunting resistances along a critical percolation path become equal to R_Q.[46]

The prediction for destruction of superconductivity via this local mechanism is in striking contrast to what one would expect in the absence of dissipation: domination near to the quantum phase transition by *collective* long-wavelength quantum fluctuations rather than local physics. In addition to the nature of the transition, *where* it would be expected to occur as parameters of the system are varied, is strikingly different for the two pictures. The long-wavelength quantum fluctuations should be controlled by the interplay between the Josephson couplings among grains and the Coulomb interactions, the former acting to decrease the phase fluctuations and the latter to decrease the charge fluctuations. If long-wavelength physics dominates, the location of the transition would thus be expected to depend markedly on the strength of the Josephson couplings. In contrast, for a single junction and by naive extension for a network of junctions, the location of the dissipation induced transition would be entirely determined by the shunting resistances, independent of the Josephson couplings.

The primary purpose of this paper is to begin to reconcile these two approaches by studying a deceptively simple system: two resistively shunted Josephson junctions coupled in series through a superconducting grain. This system, in addition to its intrinsic interest,[53] provides a simple paradigm for the competing effects of dissipation and quantum fluctuations on superconductivity.

An important simplification in all previous theoretical studies of JJ arrays is the assumption that the superconducting grains are sufficiently large that they can effectively be treated as macroscopic. In the case of several junctions in series, such an assumption leads to a result that the superconductor-to-normal transition occurs on each junction separately and takes place when the values of the individual shunting resistances are equal to the quantum of resistance $R_Q = h/(2e)^2$. In this paper we take into account the effects of finite-size grains, specifically by considering two bulk superconducting leads connected by a pair of Josephson junctions in series through a *mesoscopic* grain. We show that the

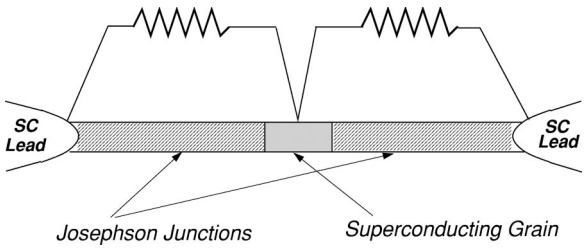

FIG. 1. A mesoscopic superconducting grain connected to superconducting leads via Josephson junctions and resistive shunts.

quantum dynamics of the two junctions, which are independent over a wide range of temperatures, become strongly coupled below a characteristic crossover temperature. In the low-temperature regime, this simple system exhibits surprisingly rich behavior, including two distinct superconducting phases. In some regimes of parameter space, the superconductor-to-normal transition between the two macroscopic leads is determined by the *total* shunting resistance of the system, rather than individual resistances of the junctions, while in other regimes its location depends on the strengths of the Josephson couplings as well as the shunting resistances. In this latter case, the corresponding critical behavior becomes very different from the single junction case.

The basic system is shown in Fig. 1. Dissipation occurs in Ohmic shunts between the superconducting contacts and the grain. Such systems may be understood in terms of a two-fluid model in which Cooper pairs tunneling across Josephson junctions represent the superfluid and electrons flowing through the shunt resistors represent the normal fluid.[54–56] The presence of two fluids in the middle grain suggests considering it as a double grain with a superconducting part and a normal part as shown in Fig. 2. We assume for simplicity that the normal and superconducting charges of the two parts experience the same electrostatic potential as they overlap in space. The chemical potentials of the two parts, however, do *not* have to be the same. When these differ, the resulting electrochemical potential difference can cause charge relaxation within the grain that will act to equilibrate its normal and superfluid components. In this paper we assume a simple

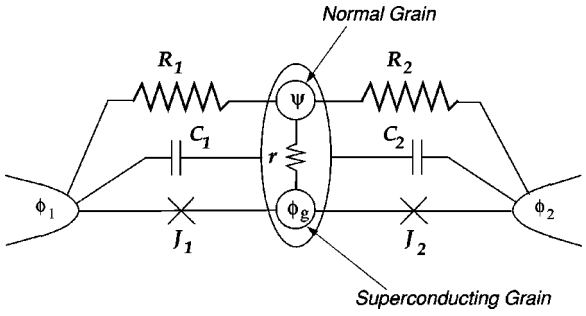

FIG. 2. Effective circuit consisting of two Josephson junctions (J_1, J_2) connecting the macroscopic electrodes (ϕ_1, ϕ_2) to a mesoscopic grain. The grain is modeled in a two-fluid manner, as a superconducting grain (ϕ_g) connected through a phenomenological resistance r to a normal-fluid grain (ψ). R_1, R_2 are the shunt resistors connecting the normal fluid of the grain to the superconducting contacts, in which the normal-superconducting relaxation is fast.

Ohmic model of this relaxation with conversion current

$$I_{ns} = \frac{V_n - V_s}{r}, \tag{1}$$

where V_n and V_s are the electrochemical potentials of the normal and superconducting fluids on the grain. The coefficient r is a phenomenological parameter of our model that we will call the conversion resistance. Decoupling of the two chemical potentials is similar to the nonequilibrium state of the superconducting and normal fluids, as discussed for phase slip centers at finite current.[57–59] We assume that the two leads are macroscopic, so that there is perfect coupling between the superconducting and normal fluids in each of them (this corresponds to the conversion resistances in the leads being negligible).

The model we arrive at using the arguments above is quite general. One could also obtain it by considering the electromagnetic modes that Cooper-pair tunneling events excite as discussed in Appendix B. This alternative approach does not require a two-fluid picture.

It is worth pointing out that our system bears some resemblance to Cooper-pair box systems studied recently in the context of quantum computing and mesoscopic qubits.[60–63] The charge on the grain could be used as the quantum number of a qubit. The biggest obstacle to quantum computation is then the limited lifetime of the quantum state of the qubit. Quantum fluctuations and interactions with the environment limit the lifetime of such a state, so practical realizations of qubits require systems with low dissipation. In this paper, in contrast, we study the Cooper-pair box system in a highly dissipative environment. Another system that resembles Fig. 2 was studied in Ref. 64 in the classical regime and was shown to exhibit interesting effects that are reminiscent of the effects we find in our model.

This paper is organized as follows. In Sec. II we present a microscopic Hamiltonian and derive the quantum action. To ascertain the consistency of this derivation we demonstrate in Appendix A that the classical equations of motion obtained from the action correspond to the electrodynamics of the circuit in Fig. 2. From the analysis of the quantum model we show the existence of a new temperature scale T^* set by the level spacing in the grain. At temperatures higher than T^* the two junctions are decoupled and can be considered separately. If the grain is macroscopic, $T^* \to 0$ and the system is always in the decoupled regime. This is the case considered in the literature thus far.[46–52] For temperatures below T^* one cannot neglect interactions between the junctions, and the effective low-temperature description is given by two coupled quantum sine-Gordon models.

In Sec. III we use renormalization group (RG) methods to analyze the two-component sine-Gordon theory in the limit of weak Josephson coupling and obtain its phase diagram. We show that the system can have five distinct phases: fully superconducting (FSC) where both junctions are superconducting; normal (NOR) where both junctions are normal and there is no phase coherence between the leads; N1-S2, where junction 1 is normal and junction 2 is superconducting; S1-N2, where junction 1 is superconducting and junction 2 is

normal; and SC*, in which Cooper pairs are localized on the grain, so individual junctions are insulating, but there is superconducting coherence between the leads due to cotunneling processes. We provide simple arguments for the phase boundaries based on electrical circuit considerations of the effective shunting resistances for various Cooper-pair tunneling events.

In Sec. IV we analyze the system in the opposite regime of strong Josephson couplings using a dual two-component sine-Gordon model and considerations of quantum phase slips. The RG analysis is again supplemented by effective shunting resistance arguments which determine the action of the various quantum phase slip processes. It is found that the phase diagrams obtained in the weak- and strong-coupling limits differ in the location of the NOR to FSC phase boundary.

In Sec. V we show that the difference between strong- and weak-coupling phase diagrams signals the existence of a novel regime with the fully normal to fully superconducting transition controlled by a critical fixed point at intermediate Josephson coupling. We analyze the appropriate fixed point, whose properties depend continuously on the resistances, and discuss the RG flow in its vicinity.

In Sec. VI we explore the surprisingly rich symmetries of the two-junction system. In addition to a weak-to-strong duality, the system also exhibits a permutation triality that implies that aspects of the phase diagram are invariant under interchange of any of the three resistances involved in the dissipative transport.

In Sec. VII we review some experimental implications of our work and discuss such questions as observation of the crossover temperature scale T^*, experimental identification of the novel superconducting phase SC*, and universality of the resistance at the superconductor-to-normal transition. We also suggest that our results may be relevant for understanding some puzzling experimental results on superconductor-to-normal transitions in thin wires and films.

Finally, in Sec. VIII we summarize the main results. To maintain the coherence of the presentation we delegate most of the technical calculations to appendixes. In particular, the renormalization group analysis of the two-component sine-Gordon model and the relations to classical Coulomb gasses are given in Appendixes D (weak coupling), and E (strong coupling).

II. MICROSCOPIC MODEL

A. Hamiltonian of the two-junction system

The system we wish to describe consists of a mesoscopic superconducting grain situated between two macroscopic superconducting leads (Fig. 2). The grain interacts with the leads both electrostatically and through a weak link. The electrostatic interaction is capacitative while the weak link allows the flow of both Cooper pairs and normal electrons. Cooper pairs flow through a Josephson junction from the superconducting part of the grain to the leads. Normal electrons flow from the normal part of the grain to the leads through what we model as a shunt resistor.

In order to understand the quantum dynamics of this system we must first obtain an appropriate low-energy effective Hamiltonian. This should include the charging energy for the grain and leads, the Josephson coupling energies for the junctions, and appropriate Hamiltonians for the shunt resistors which can be approximated by heat baths.[34,35]

The charging energy of the system includes both electrostatic and electrochemical capacitances. All the islands (here we use the term island to denote either the electrodes or the grain) have part of their charge Q_{Si} in the form of superconducting Cooper pairs and part of their charge Q_{Ni} in the form of normal fluid. Both kinds of charge contribute to the electrostatic potential and have their own compressibility. The electrochemical potentials for the superconducting and normal electrons on island i are

$$V_{Si}=\varphi_i+D_{Si}Q_{Si},$$

$$V_{Ni}=\varphi_i+D_{Ni}Q_{Ni}. \tag{2}$$

The index i is summed over electrodes 1, 2, and the grain g, φ_i is the electric potential, D_i's are the inverse of the compressibilities of the fluids S and N in a noninteracting approximation, and e^2D_{Ni} is the level spacings of the normal electrons in the island i.[65] The electrostatic potential on island i is related to the charges on all the islands via the capacitance matrix C_{ij}:

$$\varphi_i=\sum_j C_{ij}^{-1}(Q_{Sj}+Q_{Nj}). \tag{3}$$

Hence, for the electrochemical potentials we have

$$V_{Si}=\sum_j (\kappa_{Sij}^{-1}Q_{Sj}+C_{ij}^{-1}Q_{Nj}),$$

$$V_{Ni}=\sum_j (C_{ij}^{-1}Q_{Sj}+\kappa_{Nij}^{-1}Q_{Nj}), \tag{4}$$

where we defined

$$\kappa_{Sij}^{-1}=C_{ij}^{-1}+D_{Si}\delta_{ij},$$

$$\kappa_{Nij}^{-1}=C_{ij}^{-1}+D_{Ni}\delta_{ij}, \tag{5}$$

with δ_{ij} a Kronecker delta. By integrating out the electrochemical potentials in Eqs. (4) we find the charging part of the Hamiltonian

$$\mathcal{H}_Q=\frac{1}{2}\sum_{ij}\kappa_{Sij}^{-1}Q_{Si}Q_{Sj}+\frac{1}{2}\sum_{ij}\kappa_{Nij}^{-1}Q_{Ni}Q_{Nj}$$

$$+\sum_{ij}C_{ij}^{-1}Q_{Si}Q_{Nj}. \tag{6}$$

At this point we introduce superconducting phases ϕ_i on the islands and "normal phases" ψ_i, which we define formally to be conjugate to Q_{Ni} (Ref. 43):

$$[Q_{Ni},\psi_j]=-ie\delta_{ij} \quad [Q_{Si},\phi_i]=-2ie\delta_{ij},$$

$$[Q_{Ni},\phi_i]=0, \quad [Q_{Si},\psi_j]=0. \tag{7}$$

By using Eqs. (6) and (7), it is easy to verify that the Heisenberg equations of motion for the two phases give the correct Josephson relations

$$\frac{\hbar}{2e}\frac{d\phi_i}{dt}=\frac{i}{2e}[\mathcal{H}_Q,\phi_i]=V_{Si},$$

$$\frac{\hbar}{e}\frac{d\psi_i}{dt}=\frac{i}{e}[\mathcal{H}_Q,\psi_i]=V_{Ni}. \tag{8}$$

The other important energies involving the superconducting degrees of freedom are the Cooper-pair tunnelings, with

$$\mathcal{H}_J=-J_1\cos(\phi_g-\phi_1)-J_2\cos(\phi_2-\phi_g). \tag{9}$$

The dissipation in the ohmic shunts, R_1, R_2, and the internal charge relaxation r are modeled following Caldeira and Leggett (see Refs. 36,42, and 43 for a review). In this approach, the shunting resistances are replaced by collections of harmonic oscillators (heat baths), with appropriately chosen spectral functions:

$$\mathcal{H}_{dis}=\mathcal{H}_{bath}(R_1,2\psi_1-2\psi_g)+\mathcal{H}_{bath}(R_2,2\psi_2-2\psi_g)+\mathcal{H}_{bath}(r,\phi_g-2\psi_g). \tag{10}$$

We will not give the explicit form of the appropriate Hamiltonians here, but in the next subsection we give the effective actions obtained after integrating out the heat-bath degrees of freedom. The heat-bath model is the simplest quantum model that gives the correct classical equations of motion for systems with dissipation. Later in this paper we will discuss some of its drawbacks; however, we believe that it gives a qualitatively correct picture for a general mechanism of dissipation.

Collecting all the terms, we obtain an effective Hamiltonian that describes the system shown in Fig. 2:

$$\mathcal{H}(Q_{Ni},Q_{Si},\phi_i,\psi_i)=\mathcal{H}_Q+\mathcal{H}_J+\mathcal{H}_{dis}. \tag{11}$$

B. Imaginary-time action

From the Hamiltonian (11) and commutation relations (7), we can construct the imaginary time action and partition function for the system in Fig. 2:

$$Z=\int \mathcal{D}Q_{Ni}\mathcal{D}Q_{Si}\mathcal{D}\phi_i\mathcal{D}\psi_i\exp(-S),$$

$$S=-\frac{i}{2e}\sum_i\int_0^\beta d\tau Q_{Si}\dot{\phi}_i-\frac{i}{e}\sum_i\int_0^\beta d\tau Q_{Ni}\dot{\psi}_i+\int_0^\beta d\tau\mathcal{H}(Q_{Ni},Q_{Si},\phi_i,\psi_i). \tag{12}$$

It is important to point out that in the presence of Ohmic dissipation the phase variables ϕ_i and ψ_i should be periodic at $\tau=0$ and $\tau=\beta$ with *no phase twists* by multiples of 2π allowed. This follows from the fact that a 2π phase twist causes dissipation and is thus measurable. The Ohmic dissipation allows continuous charge transfer (as opposed to transfer of multiples of e) from the shunting resistors to the grain. Therefore any noninteger charge induced by the gate voltage can be screened out. (For a more detailed discussion see Refs. 43 and 66). This potential drawback of the Caldeira-Leggett model of dissipation may be overcome if one introduces a more complicated form of dissipation, such as via quasiparticle tunneling (see, e.g., Ref. 43).

The quantum action in Eqs. (12) is quadratic in Q_{Si} and Q_{Ni}, so they may be integrated out (for details, see Appendix A1). The electrochemical contribution is (in terms of the electrochemical potentials)

$$S_Q=\int_0^\beta d\tau\frac{1}{2(2e)^2}\left(\sum_i C_{Qi}(V_{Si}-V_{Ni})^2+\sum_{ij}(s_iV_{Si}+\eta_iV_{Ni})C_{ij}(s_jV_{Sj}+\eta_jV_{Nj})\right). \tag{13}$$

This is very easy to interpret. The level spacings give rise to the first term in the brackets, making a potential difference between the two fluids on one island energetically costly. The second term in the brackets is the charging energy one would expect from a conventional system of islands, but the potential on each island is replaced by a weighted average of the normal-fluid potential and the superfluid potential: $\overline{V_i}=s_iV_{Si}+\eta_iV_{Ni}$.

In terms of the phase variables, the full action can be written as

$$Z=\int \mathcal{D}\phi_i\mathcal{D}\psi_i\exp(-S_Q-S_J-S_{dis})$$

$$S_Q=\int_0^\beta d\tau\frac{1}{2(2e)^2}\left(\sum_i C_{Qi}(\dot{\phi}_i-2\dot{\psi}_i)^2+\sum_{ij}(s_i\dot{\phi}_i+\eta_i2\dot{\psi}_i)C_{ij}(s_j\dot{\phi}_j+\eta_j2\dot{\psi}_j)\right),$$

$$S_J=\int_0^\beta d\tau[-J_1\cos(\phi_g-\phi_1)-J_2\cos(\phi_2-\phi_g)],$$

$$S_{dis}=\beta\sum_{\omega_n}\frac{R_Q}{4\pi}\left(\frac{|\omega_n|}{R_1}|2\psi_{1,(\omega_n)}-2\psi_{g,(\omega_n)}|^2+\frac{|\omega_n|}{R_2}|2\psi_{2,(\omega_n)}-2\psi_{g,(\omega_n)}|^2+\frac{|\omega_n|}{r}|\phi_{g,(\omega_n)}-2\psi_{g,(\omega_n)}|^2\right), \tag{14}$$

where the Matsubara frequencies are $\omega_n=2\pi Tn$, and we have defined $C_{Qi}=(D_{Si}+D_{Ni})^{-1}$, $s_i=D_{Ni}/(D_{Si}+D_{Ni})$, and $\eta_i=D_{Si}/(D_{Si}+D_{Ni})$.

An important consequence of the domain of the phase fields ϕ_g and ψ being the real line rather than a circle is that the Berry phase has no effect on the behavior of the system.

A Berry phase could arise if we included the gate voltage effects in Eqs. (2) and (6) by shifting $Q_{Sg}\rightarrow Q_{Sg}-Q_0$, which would lead to additional terms in the action (13) of the form $iQ_0\int_0^\beta \dot{\phi}_g$. But because 2π phase twists are not allowed, the additional action vanishes due to the periodic boundary conditions in imaginary time.

As a consistency check of the action (14), we demonstrate in Appendix A2 that its real-time equivalent gives rise to equations of motion that coincide exactly with the basic electrodynamic equations for the circuit in Fig. 2.

In this paper we consider the limit of macroscopic electrodes, so we can set the corresponding $D_1=D_2=0$ on these. The first term in Eq. (13) then imposes perfect coupling between the superconducting and normal fluids in the electrodes, i.e., $\phi_1=2\psi_1$ and $\phi_2=2\psi_2$. Note that this assumption does not restrict us to taking an infinite capacitance for the electrodes: the inverse of the level spacing grows as the volume of the grains, whereas capacitances increase only linearly with the dimensions. We restrict our discussion to the case when the largest capacitances in the system are the *mutual capacitances* between the electrodes and the grain, C_1 and C_2, for electrodes 1 and 2 respectively. In Appendix A3 we show that in this case the charging part can be simplified if we introduce the phase difference variables

$$\Delta_1=\phi_g-\phi_1,$$

$$\Delta_2=\phi_2-\phi_g,$$

$$\Delta_g=\phi_g-2\psi_g, \tag{15}$$

and the center-of-mass variable Φ,

$$\Phi=\frac{C_{11}+C_{12}+C_{1g}}{C_{tot}}\phi_1+\frac{C_{22}+C_{12}+C_{2g}}{C_{tot}}\phi_2 + \frac{C_{1g}+C_{2g}+C_{gg}}{C_{tot}}s_g\phi_g+\frac{C_{1g}+C_{2g}+C_{gg}}{C_{tot}}\eta_g 2\psi_g, \tag{16}$$

where

$$C_{tot}=\sum_{ij} C_{ij} \tag{17}$$

(note that C_{tot} is not affected by the mutual capacitances C_1 and C_2 but is determined by the capacitance of the system to the ground). We thus have

$$S_Q=\frac{1}{2(2e)^2}\int_0^\beta d\tau[C_1(-\dot{\Delta}_1+\eta_g\dot{\Delta}_g{}^2 + C_2(\dot{\Delta}_2+\eta_g\dot{\Delta}_g)^2+C_Q\dot{\Delta}_g^2+C_{tot}\dot{\Phi}^2. \tag{18}$$

The center-of-mass coordinate Φ completely decouples from the phase differences in the charging part of the action, and it is not present in S_J and S_{dis}; these can be written as

$$S_J=\int_0^\beta d\tau[-J_1\cos(\Delta_1)-J_2\cos(\Delta_2)],$$

$$S_{dis}=\beta\sum_{\omega_n}\frac{R_Q}{2\pi}\left(\frac{|\omega_n|}{R_1}|\Delta_{1,(\omega_n)}+\Delta_{g,(\omega_n)}|^2+\frac{|\omega_n|}{R_2}|\Delta_{2,(\omega_n)} + \Delta_{g,(\omega_n)}|^2+\frac{|\omega_n|}{r}|\Delta_{g,(\omega_n)}|^2\right). \tag{19}$$

Therefore the center-of-mass coordinate Φ factors out in the partition function. From Eqs. (18) and (19) we see that Δ_g appears quadratically in the action and can be integrated out. After this integration and also after neglecting terms involving $C_1/C_Q, C_2/C_Q \ll 1$, we obtain

$$S=\frac{R_Q}{2\pi}\beta\sum_{\omega_n}\left[|\Delta_{1,(\omega_n)}|^2\left(\frac{|\omega_n|}{2R_1}\frac{\left[\frac{\hbar}{C_Q}\left(\frac{1}{r}+\frac{1}{R_2}\right)+|\omega_n|+C_1R_1\omega_n^2/\hbar\right]}{\left[\frac{\hbar}{C_Q}\left(\frac{1}{R_1}+\frac{1}{R_2}+\frac{1}{r}\right)+|\omega_n|\right]}\right) + |\Delta_{2,(\omega_n)}|^2\left(\frac{|\omega_n|}{2R_2}\frac{\left[\frac{\hbar}{C_Q}\left(\frac{1}{r}+\frac{1}{R_1}\right)+|\omega_n|+C_2R_2\omega_n^2/\hbar\right]}{\left[\frac{\hbar}{C_Q}\left(\frac{1}{R_1}+\frac{1}{R_2}+\frac{1}{r}\right)+|\omega_n|\right]}\right) + \Delta_{1,(\omega_n)}\Delta_{2,(-\omega_n)}\frac{|\omega_n|}{R_1R_2}\frac{\hbar/C_Q(1+|\omega_n|\eta_gC_1R_1/\hbar)(1+|\omega_n|\eta_gC_2R_2/\hbar)}{\left[\frac{\hbar}{C_Q}\left(\frac{1}{R_1}+\frac{1}{R_2}+\frac{1}{r}\right)+|\omega_n|\right]}\right]+S_J. \tag{20}$$

Looking at the ubiquitous denominators of Eq. (20) we notice the expression

$$\frac{\hbar}{C_Q}\left(\frac{1}{r}+\frac{1}{R_1}+\frac{1}{R_2}\right)+|\omega_n|.$$

The scale for the Matsubara frequencies ω_n is set by temperature; hence a new temperature scale emerges from Eq. (20):

$$T^*=(2e)^2(D_S+D_N)R_Q\left(\frac{1}{r}+\frac{1}{R_1}+\frac{1}{R_2}\right). \tag{21}$$

This is the level spacing on the grain ($1/C_Q=D_S+D_N$) times a dimensionless resistance-dependent factor, and it is also of the order of the inverse escape time from the grain.

High-temperature limit. When $T\gg T^*$ the denominator in Eq. (20) is dominated by $|\omega|\gg T^*$, and the effective action for high temperatures is

$$\begin{aligned}S\approx&\frac{R_Q}{2\pi}\beta\sum_{\omega_n}\left[\frac{1}{2}|\Delta_{1,(\omega_n)}|^2\left(\frac{|\omega_n|}{R_1}+C_1\omega_n^2/\hbar\right)\right.\\&+\frac{1}{2}|\Delta_{2,(\omega_n)}|^2\left(\frac{|\omega_n|}{R_2}+C_2\omega_n^2/\hbar\right)+\Delta_{1,(\omega_n)}\Delta_{2,(-\omega_n)}\frac{|\omega|}{R_1R_2}\\&\left.\times\left(\frac{\hbar/C_Q(1+|\omega_n|\eta_gC_1R_1/\hbar)(1+|\omega_n|\eta_gC_2R_2/\hbar)}{|\omega|}\right)\right]\\&+S_J.\end{aligned} \tag{22}$$

In this limit we see that the interaction term between the two junctions (which is T independent to leading order in C_1/C_Q, C_2/C_Q) is negligible compared to the other resistive and capacitative parts of the action; the two junctions are thus effectively decoupled for $T\gg T^*$. The dissipations for the two junctions in this limit are set simply by the individual shunt resistances R_1 and R_2. This is the limit that has been discussed in the literature; its validity at low temperatures relies on the basic assumption of *macroscopic* grains, for which $T^*=0$.

Low-temperature limit. At temperatures T below T^* [we assume that $T^*<\hbar/(R_1C_1)$ and $T^*<\hbar/(R_2C_2)$] a qualitatively different picture emerges in which the coupling between the two junctions becomes important. The low-energy effective theory is

$$Z\approx\int\mathcal{D}\Delta_1\mathcal{D}\Delta_2e^{-S_d-S_C-\tilde{S}_J},$$

$$\tilde{S}_J=\int_0^\beta d\tau[-J_1\cos(\Delta_1)-J_2\cos(\Delta_2)-J_+\cos(\Delta_1+\Delta_2)],$$

$$S_C=\beta\sum_{\omega_n}\left(\frac{C_Q}{2(2e)^2}\left|\frac{rR_2\Delta_1+rR_1\Delta_2}{rR_1+rR_2+R_1R_2}\right|^2\omega_n^2\right),$$

$$S_d=\beta\sum_{\omega_n}\frac{|\omega_n|}{2}\vec{\Delta}^\dagger\hat{G}\vec{\Delta}, \tag{23}$$

with

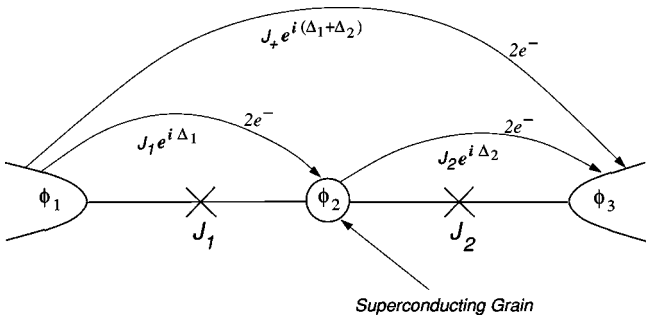

FIG. 3. Physical interpretation of expanding the $J_i\cos\Delta_i$ terms in the action (23). The weak Josephson coupling action can be mapped to a theory of interacting Cooper-pair tunneling events (Coulomb-gas representation) with each pair-tunnel "charge" corresponding to a Cooper pair transferred through one of the junctions. The cotunneling events which transfer Cooper pairs from lead to lead are also shown; in the Coulomb-gas representation these correspond to pair-tunnel dipoles.

$$\vec{\Delta}\equiv(\Delta_1,\Delta_2) \tag{24}$$

and the matrix

$$\hat{G}=\frac{R_Q}{2\pi Y}\begin{pmatrix}r+R_2 & r\\ r & r+R_1\end{pmatrix}, \tag{25}$$

where

$$Y\equiv rR_1+rR_2+R_1R_2. \tag{26}$$

In the equations above we have added, for future purposes, a lead-to-lead Josephson coupling term representing cotunneling processes via the grain. This term describes a Cooper-pair tunneling (pair-tunnel event) from the left electrode to the right electrode (see Fig. 3) via a virtual intermediate state with an additional pair on the grain. Such processes appear perturbatively at second order in J_1 and J_2 and will be generated in the RG flows for the action (23) [see discussion below Eq. (27)].

It is important to note that level spacing $D_g=D_{sg}+D_{ng}$ only appears in S_C via the quantum capacitance $C_Q=D_g^{-1}$, whose precise form will not matter except to yield a high-frequency cutoff. By the same token, a different form of the capacitative energy of the leads and grains would only modify S_C and not change any of the analysis presented in this paper.

Action (23) is one of the main results of this paper, and in the following sections we will mostly be concerned with studying its properties.

III. WEAK-COUPLING ANALYSIS

In this section we analyze the low energy properties of the system in the weak-Josephson-coupling limit.

A. Renormalization group equations

In the limit of weak Josephson couplings $\{J_i\}$, the quantum action (23) can be analyzed directly in the generalized

sine-Gordon representation. In Appendix D2, RG flow equations are derived to second order in the Josephson couplings:

$$\frac{dJ_1}{dl} = J_1\left(1 - \frac{R_1 + r}{R_Q}\right) + \frac{R_2}{R_Q} J_2 J_+ ,$$

$$\frac{dJ_2}{dl} = J_2\left(1 - \frac{R_2 + r}{R_Q}\right) + \frac{R_1}{R_Q} J_1 J_+ ,$$

$$\frac{dJ_+}{dl} = J_+\left(1 - \frac{R_1 + R_2}{R_Q}\right) + \frac{r}{R_Q} J_1 J_2 . \tag{27}$$

In writing these we have set a combination of the short-time cutoffs to be equal to 1. In physical units, the energy cutoff is of the order of the charge relaxation rate of the junctions in units of which we are here measuring the $\{J_i\}$. The first-order terms in the RG flows arise, as usual, from integrating out fast modes in the quadratic part of action (23). The second-order terms are obtained from recombinant terms in the expansion in powers of J's of Eq. (23). These can be understood physically; pair-tunnel events on junctions 1 and 2 can combine to form a cotunneling event between the two leads, while a cotunneling event plus a pair tunnel in the opposite direction across one of the junctions is equivalent to pair tunneling across the other junction (for details see Appendix). From Eqs. (27) we see that, as claimed in the previous section, J_+ gets generated at low energies even if we start with a model in which $J_+ = 0$.

B. Weak-coupling phase diagram

Surprisingly, the simple flow equations (27) give rise to five different regimes. When all J's are irrelevant about the uncoupled fixed line so that they flow to zero, the system is in the normal state with no supercurrents between the leads or between either lead and the grain. This *normal* (NOR) phase occurs if R_1 and R_2 are both sufficiently large. When all J's are relevant and grow under the RG flows, the systems is in a fully superconducting phase that we denote FSC. This occurs if all the resistances are sufficiently small. For intermediate ranges of the resistances, the situation is more complicated.

When only one out of the three J's is relevant while the other two flow to zero at low energies, the system is in a ''mixed phase''; as we shall see, there are three such phases. When the only relevant coupling is J_1, junction 1 is superconducting, and junction 2 is normal, we call this phase S1-N2. With respect to lead-to-lead transport this is like the normal phase. Analogously we will have an N1-S2 phase when J_2 is relevant but J_1 and J_+ are not. Rather surprisingly, there can also be a situation in which J_+ is relevant but J_1 and J_2 are not. This is a phase in which individual junctions are normal, but the circuit as a whole is superconducting and Cooper pairs can flow freely between the leads. We denote this phase SC*. Physically, it corresponds to Cooper pairs being localized on the grain, so that the individual junctions are normal; however, the cotunneling processes, via virtual Cooper-pair excitations on the grain, induce superconducting coherence between the leads. A similar phase was discussed by Korshunov[50,51] and Bobbert *et al.*[52] in the context of one-dimensional Josephson junction arrays.

Inspection of the flow equations shows that as long as $R_1, R_2, r > 0$ there *cannot* be phases in which two of the three J's grow while the third flows to zero: the coupling terms in Eqs. (27) from the two growing ones will drive the third J to grow as well. The system will then be in the *fully superconducting* (FSC) phase.

To lowest order for small J's, the phase boundaries between these phases are set by the relevance of J_1, J_2, and J_+ about the decoupled (normal) fixed line; these are determined by the combinations $R_1 + r$, $R_2 + r$, and $R_1 + R_2$ respectively.

This simple analysis, however, is not sufficient to obtain the correct phase diagram. In the regions where one of the three couplings J_1, J_2, or J_+ is relevant, Eqs. (27) no longer apply, since they are derived for small J's.

For instance, the N1-S2-to-FSC transition line needs to be calculated bearing in mind that J_2 is relevant. A better approximation for this transition is obtained by noting that the fluctuations in phase difference across junction 2, Δ_2, will be small in the N1-S2 phase. Thus in this regime we can approximately set $\Delta_2 = 0$ in Eq. (23). This modifies the RG flow for J_1 to

$$\frac{dJ_1}{dl} = J_1\left(1 - \frac{R_1 + \dfrac{rR_2}{r + R_2}}{R_Q}\right). \tag{28}$$

[We will see later that in the Coulomb gas language, Eq. (28) corresponds to including the screening effects of unbound type 2 charges when considering the unbinding transition for charges of type 1 (see Appendix D2 for details).] From Eq. (28) we find that the N1-S2-to-FSC boundary gets shifted to

$$R_1 + \frac{rR_2}{r + R_2} = R_Q . \tag{29}$$

Similar modifications of the phase boundaries appear for all transitions that involve ordering of one field in the presence of order in another: S1-N2 to FSC (ordering of Δ_2 when Δ_1 is ordered) and SC* to FSC (ordering of Δ_1 and Δ_2 when $\Delta_1 + \Delta_2$ is ordered).

The correct—and rather complicated—weak-coupling phase diagram is shown in Fig. 4. A particularly interesting regime occurs for $r > R_Q$. In this regime the two junctions cease to behave as such; instead, they behave much like a single junction shunted by the total resistance, $R_1 + R_2$, which therefore determines the location of the superconducting-to-normal transition between the two leads. This will be discussed further in Sec. VII.

C. Circuit theory for weak coupling

In this subsection we show how the phase diagram of Fig. 4 can be obtained by simple physical arguments. Before proceeding it is useful to recall such an argument for a single junction.

We want to investigate the stability of the superconducting state of a single Josephson junction with an Ohmic shunt.

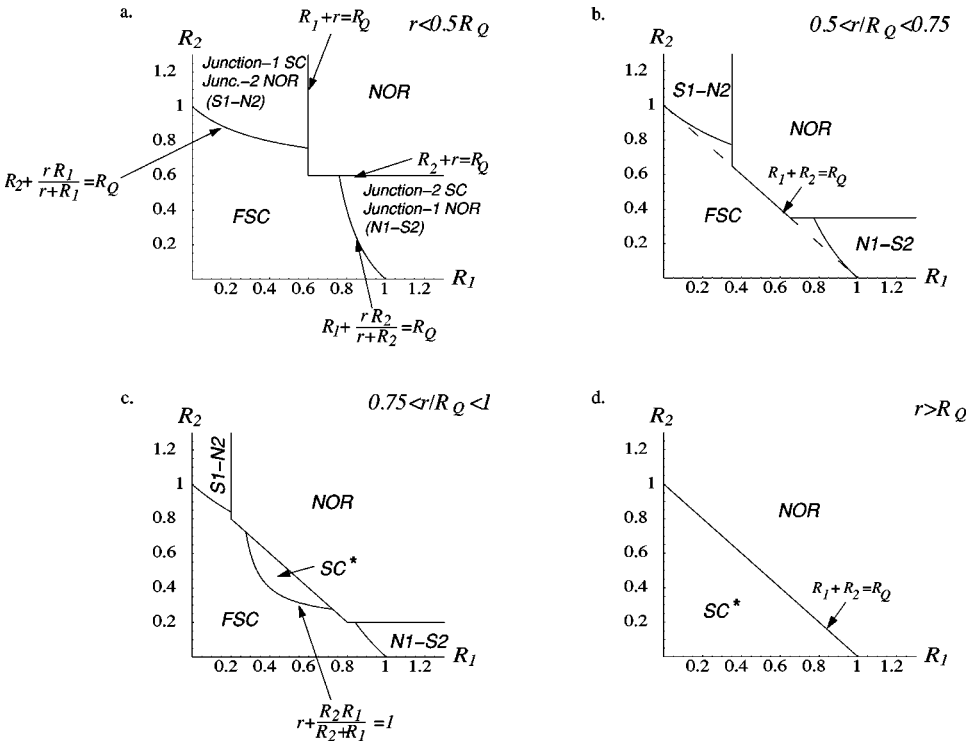

FIG. 4. Weak-Josephson-coupling phase diagram. Phase boundary formulas apply everywhere, although they are each given in only one graph. (a) When $r<0.5R_Q$ four of the five phases are present; each junction is either normal or superconducting. (b) For larger r, the shape of the phase boundary between the FSC and NOR phases changes. (c) When $0.75<r/R_Q<1$ the SC* appears and all five phases are present. (d) When $r>R_Q$ only SC* survives of the mixed phases, and FSC disappears.

In the superconducting phase, Cooper-pairs are delocalized between the leads. Each Cooper-pair tunneling event changes the charge on the junction by $2e$. This charge needs to be screened by the normal electrons in the shunt, thereby causing a voltage drop to appear across the junction. By the Josephson relation, this voltage drop induces a change in the phase difference across the junction. The superconducting phase with delocalized Cooper pairs will survive only when the phase change due to one Cooper-pair tunneling event is less than 2π (otherwise the phase becomes delocalized). From circuit equations and the Josephson relation we find

$$2e=\int I_N dt=\int \frac{\Delta V}{R_S}dt=\frac{\hbar}{2eR_S}\int \frac{d\phi}{dt}dt=\frac{\hbar}{2eR_S}\Delta\phi, \tag{30}$$

where I_N is the normal screening current, ΔV is the voltage difference across the junction, and $\Delta\phi$ is the phase change due to a Cooper tunneling. Rewriting the last relation as

$$\frac{\Delta\phi}{2\pi}=\frac{R_S}{R_Q}, \tag{31}$$

we obtain the usual condition; the shunted Josephson junction is superconducting when $R_S<R_Q$. We can summarize this argument by saying that a Cooper-pair tunneling event provides a current source with a magnitude that depends on the shunting resistance. By the Josephson relation, this leads to a phase fluctuation across the junction, and the superconducting phase is only stable when this phase fluctuation is less than 2π. (Note that this argument does not really yield the exact condition: a multiplicative factor of order unity could have arisen. A fuller analysis, as from the RG flows, is needed to obtain the correct coefficient.)

Applying this approach to the two-junction system of Fig. 2 effectively reduces the problem to determining the effective shunting resistance associated with Cooper-pair tunneling events in various situations. As in the single junction case, a Cooper-pair tunneling can be simply modeled as a *current source*.

(i) To find the transition between S1-N2 and the NOR phase, consider a Cooper-pair tunneling across junction 1 with junction 2 insulating and acting as a circuit disconnect. The effective resistance that makes a circuit with the current source is then R_1+r [see Fig. 5(a)], and the phase boundary is at $R_1+r=R_Q$. Analogously for the N1-S2 to NOR transition we have the circuit shown in Fig. 5(b) and a phase boundary at $R_2+r=R_Q$.

(ii) The SC* to NOR transition is marked by the prolif-

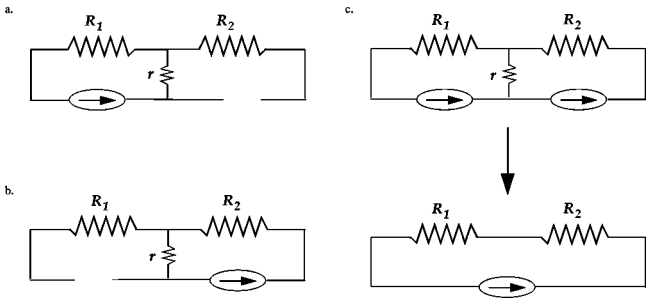

FIG. 5. Effective circuits for pair tunneling events. A pair tunnel corresponds to a current source, whereas a junction without pair tunneling acts as an open circuit. (a) Effective circuit for a pair tunneling through junction 1. (b) Effective circuit for a pair tunneling through junction 2. (c) Effective circuit for a coherent lead-to-lead pair tunneling event. Since the current through junctions 1 and 2 is the same, the resistance r is effectively disconnected in this case.

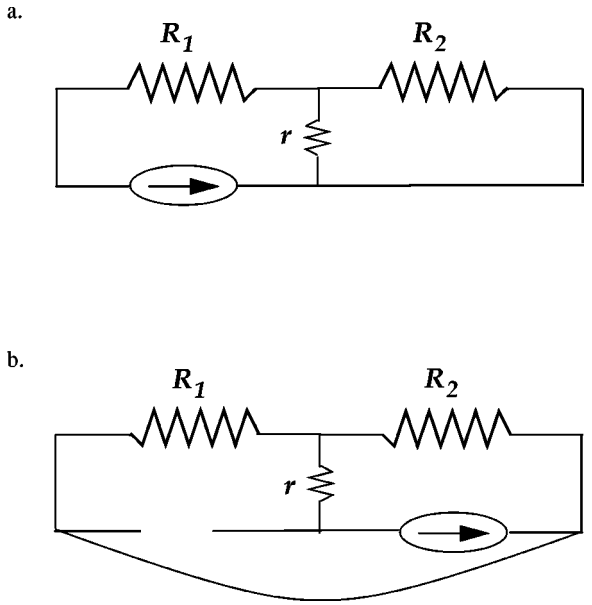

FIG. 6. (a) Effective circuit for a pair tunneling through junction 1 when junction 2 is superconducting (J_2 is relevant about the weak-coupling limit). (b) Effective circuit for a pair tunneling event through junction 1 (or 2) when J_+ is relevant and coherent lead-to-lead pair tunneling events proliferate.

eration of cotunneling processes in which a Cooper pair moves between the leads, but with both junctions individually insulating. The circuit describing this case is depicted in Fig. 5(c), with the cotunneling process described as two current sources forcing the same current through both Josephson junctions. The cotunneling process leaves no charge on the grain and is hence screened only by normal currents flowing in the resistors R_1 and R_2. The effective shunting resistance in this case is R_1+R_2 and the phase boundary is at $R_1+R_2=R_Q$.

(iii) The transition between N1-S2 and FSC occurs while junction 2 is already superconducting and can hence be replaced by a short in the circuit [see Fig. 6(a)]. The effective shunting resistance across junction one then involves r and R_2 in *parallel*, as well as R_1; therefore the phase boundary for this transition occurs at $R_1+rR_2/(r+R_2)=R_Q$. By the same token the transition between S1-N2 and FSC takes place when $R_2+rR_1/(r+R_1)=R_Q$.

(iv) To understand the FSC-to-SC* transition we need to consider the regime in which cotunneling maintains coherence between the leads; therefore these are effectively connected by a short in the circuit as shown in Fig. 6(b). Now consider a Cooper-pair tunneling from the grain to one of the leads—say, 2. The effective resistance seen by a tunneling Cooper pair is $r+R_1R_2/(R_1+R_2)$ and the phase boundary is hence at $r+R_1R_2/(R_1+R_2)=R_Q$. The effective shunt resistance for tunneling from the grain to lead 1 is the same. The nature of the SC* phase is as follows: Cooper-pair tunneling events scramble phases across junctions 1 and 2 too much for the junctions to be coherent, so Cooper pairs become localized on the grain. Nevertheless, cotunneling events allow Cooper pairs to move between the leads, so there is a well-defined phase difference between them that acts as a short between the two macroscopic leads as far as dissipation across the individual junctions.

(v) The FSC to NOR transition line is, naively, a continuation of the S1-N2-to-NOR and N1-S2-to-NOR lines. This suggests that when considering fluctuations of the phase difference across junction 1, we assume junction 2 to be insulating and vice versa. The consistency of such an approximation is highly questionable and reflects the limit of small J's as our starting point: by a weak-coupling analysis: for a weak-coupling limit to be valid, we should only approach phase boundaries from normal phases of the junction under consideration.

It is worth pointing out that in all cases described above, the effective dissipation is *decreased* relative to that in the high-temperature action (22). The most extreme case happens for the SC*-to-NOR transition which is determined by the *total* shunting resistance at low temperatures rather than individual resistances R_1 and R_2, which would determine the transitions between macroscopic grains. In the SC* phase the whole system behaves as a single junction, and the dissipation is determined by the resistance across the whole of the system.

IV. STRONG-COUPLING ANALYSIS

We have seen that much can be concluded from the weak-Josephson-coupling analysis, in particular the nature of the five possible phases and some of the transitions between them. Yet some of the transitions could only be understood via a hybrid analysis involving some large and some small couplings, and as pointed out above, the FSC to NOR transition cannot be analyzed in a controlled manner from a weak-coupling analysis. Even to solidify the identification of all of the superconducting phases, we really need to go beyond weak coupling: as soon as one or more of the J's grows without bound, the system flows out of the regime of validity of the RG flow equations used thus far and we must ask where it flows to.

In this section we turn to the limit of large Josephson coupling and attempt to analyze the phases, phase diagram, and transitions in that limit.

A. Sine-Gordon action for quantum phase slips

When the Josephson couplings are large, the system is usually in the vicinity of one of the classical minima of the Josephson potentials so that $\Delta_1\approx 2\pi n_1$, $\Delta_2\approx 2\pi n_2$ with n_1 and n_2 integers. Only rarely does the system undergo a tunneling event in which one or both of the phases winds by 2π. Such phase tunneling processes between minima of the classical potential are *quantum phase slips* (QPS's).[43] When QPS's across it are suppressed at low temperatures a Josephson junction is superconducting, but when they proliferate the junction is incapable of supporting supercurrents and becomes normal.

In weak coupling we analyzed the low-energy action in terms of Cooper-pair tunneling events. As discussed in Appendix B, this is equivalent to a classical Coulomb gas with two types of charges corresponding to pair tunneling events

through the two junctions; dissipation gives rise to effective logarithmic interactions among these. Various of the superconductor-to-normal transitions can be described as binding-unbinding transitions of this two component plasma.

In the strong-coupling case we can write a Coulomb gas representation for the quantum phase slips instead of the Cooper-pair tunneling events. The phase slips also behave as a two-component gas—phase slips on the two junctions—with logarithmic interactions between them. When the phase slips across a junction proliferate, it becomes normal; if instead their fugacity tends to zero at low-energy-scales, the junction is superconducting. Mathematically, the strong-coupling case can be analyzed by performing a Villain transformation to represent the partition function (23) in terms of two types of interacting phase slips. This classical Coulomb gas can then be transformed into a new sine-Gordon model that is *dual* to Eqs. (23). Appendix C describes the details of such transformations. We find

$$Z=\int D[\theta_1]\int D[\theta_2]\exp(-S),$$

with

$$S=\beta\sum_{\omega_n}|\omega_n|\vec{\theta}^{\,T}_{-\omega_n}\hat{M}\vec{\theta}_{\omega_n}-\int_0^\beta d\tau[\zeta_1\cos(\theta_1)+\zeta_2\cos(\theta_2)+\zeta_-\cos(\theta_1-\theta_2)], \tag{32}$$

where $\vec{\theta}=(\theta_1,\theta_2)$ and

$$\hat{M}=\hat{G}^{-1}=\frac{1}{2\pi R_Q}\begin{pmatrix} r+R_1 & -r \\ -r & r+R_2 \end{pmatrix} \tag{33}$$

is the scaled resistance matrix. The variables ζ_1,ζ_2,ζ_- are the fugacities corresponding to the three types of phase slips: ζ_1 across junction 1, ζ_2 across junction 2, and ζ_-, a combination of these that corresponds to a phase slip across 1, and a simultaneous antiphase slip across 2, thereby slipping the phase on the grain with respect to *both* of the superconducting leads.

B. Phase diagram

Following the steps leading to Eq. (27) we readily obtain the flow equations for the phase slip fugacities ζ_1,ζ_2, and ζ_-:

$$\frac{d\zeta_1}{dl}=\zeta_1\left(1-\frac{R_Q}{R_1+\dfrac{R_2 r}{R_2+r}}\right)+\frac{R_1}{Y}\zeta_2\zeta_-,$$

$$\frac{d\zeta_2}{dl}=\zeta_2\left(1-\frac{R_Q}{R_2+\dfrac{R_1 r}{R_1+r}}\right)+\frac{R_2}{Y}\zeta_1\zeta_-,$$

$$\frac{d\zeta_-}{dl}=\zeta_-\left(1-\frac{R_Q}{r+\dfrac{R_1R_2}{R_1+R_2}}\right)+\frac{r}{Y}\zeta_1\zeta_2, \tag{34}$$

where we use $Y\equiv R_1R_2+rR_1+rR_2$. These flow equations are correct to second order in the ζ's, being simply the analog of Eqs. (27) for the weak-coupling limit. We again work in units in which the short-time cutoff—here related to the ''transit time'' for a least-action phase slip—is unity.

Growth under renormalization of a fugacity ζ_i corresponds to proliferation of the corresponding QPS's and hence destruction of superconductivity across the respective junction in the case of ζ_1 or ζ_2 or between the grain and the rest of the system in the case of ζ_-.

Equation (34) gives rise, as did the weak-coupling analysis, to five phases. When all ζ's are irrelevant and flow to zero, the system is in the fully superconducting state (FSC) since isolated phase slips all cost infinite action. Conversely, if all ζ's are relevant, we expect the normal state (NOR) to obtain. As in the weak-coupling case, three mixed phases appear when only *one* of the fugacities is relevant. When ζ_1 is relevant and ζ_2 and ζ_- are not, the system is in the N1-S2 phase; analogously a relevant ζ_2 and irrelevant ζ_1 and ζ_- signal the S1-N2 phase.

If ζ_- is relevant but ζ_1 and ζ_2 are not, the special SC* phase occurs. In this phase only QPS *dipoles* proliferate; these consist of a phase slip across one junction and an *antiphase* slip across the other. Isolated phase slips across individual junctions will not occur in the SC* phase. Superconducting phase coherence between the two leads is thus *maintained*, since the phase difference between them is the sum of the phase differences for the two junctions, and a phase slip on junction 1 gets canceled by its accompanying antiphase slip on junction 2. But the phase difference between the leads and grain is ill defined in SC* as a result of the proliferated QPS dipoles. We thus see that proliferation of the QPS dipoles induces charge localization on the grain.

The transition between the two superconducting phases SC* and FSC is, from the point of view of phase slips on the individual junctions, a transition between a dipole-free state, FSC, in which all the phase slips will be bound in quadrupoles, and a phase, SC*, in which dipoles proliferate but single quantum phase slips still do not occur. Because of the free dipoles in the SC* phase, a single quantum phase slip between the two leads can consist of any combination of phase slips across the two junctions that add up to a total phase difference between the leads of 2π.

As in the weak-coupling limit (Sec. III B), we could attempt to construct a naive phase diagram showing all five phases from the *first-order* strong-coupling flow equations. This approach would give phase boundaries that depend on $R_1+R_2r/(R_2+r), R_2+R_1r/(R_1+r)$, and $r+R_1R_2/(R_1+R_2)$. But such an analysis, as in the weak-coupling limit, is not sufficient: when one type of phase slip proliferates it will partially screen the interactions between the other types of phase slips.

To do better we must consider the effects of the relevance of a $\zeta\cos\theta$ term: this will cause the dual phase θ associated with the proliferating phase slips to become localized at an integer multiple of 2π. As the θ will then not fluctuate appreciably about this at low energies, we can set it to zero. As for weak coupling, this suppression of some of the fluctuations will change the flows of the remaining fugacities and

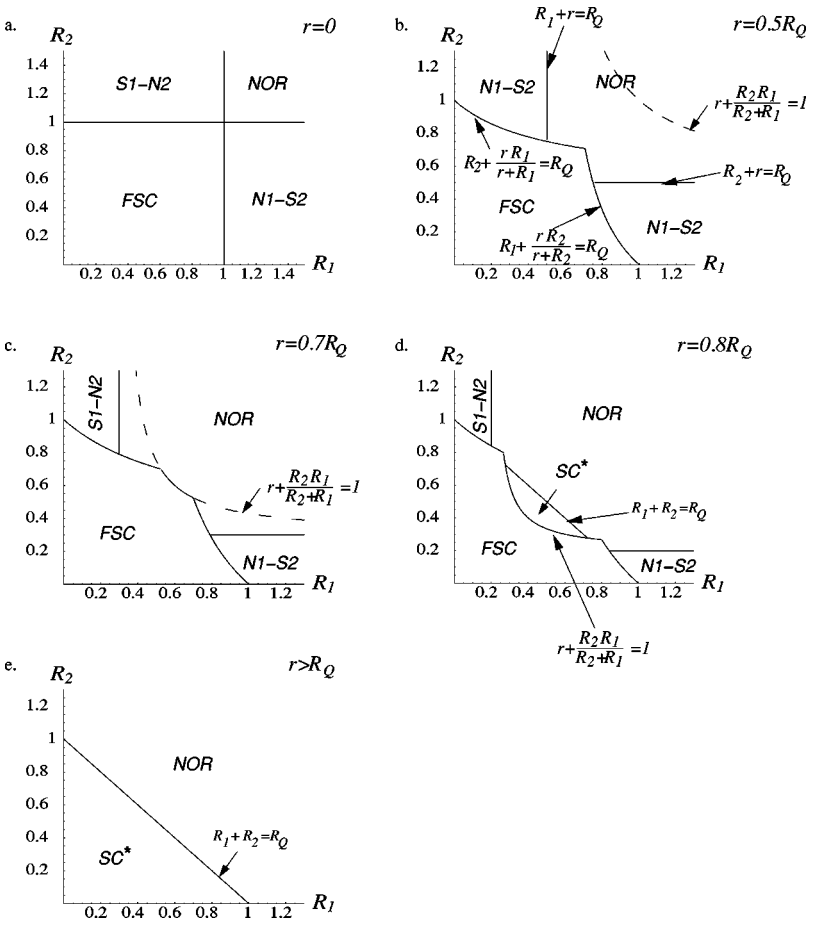

FIG. 7. Strong-Josephson-coupling phase diagram. Phase boundary formulas apply everywhere, although they are each given in only one graph. (a) $r=0$ for which the two junctions are effectively independent, (b) range $0<r/R_Q<2/3$, (c) range $2/3<r/R_Q<3/4$, (d) range $3/4<r/R_Q<1$ where all five phases are present, and (e) range $r>R_Q$ for which the two junctions act like a single junction with a shunt resistor R_1+R_2.

thereby modify the phase diagram. The complete phase diagram from such a strong-coupling analysis is shown in Fig. 7.

C. Circuit theory for strong coupling

The strong-coupling phase diagram of Fig. 7 can be simply interpreted in terms of the effective electronic circuits. Although these arguments are dual to the ones used for weak coupling, we present them here for completeness.

Again it is useful to start by considering the case of a single junction, now starting from the superconducting regime. The normal state occurs when quantum phase slips proliferate. When a QPS occurs, the phase difference across the junction changes by 2π. By the Josephson relation, this generates both a voltage drop and charge flow through the normal shunt. In the normal state the Cooper pairs should be localized; therefore, such a state can only be stable if the charge fluctuation caused by an individual QPS is less than $2e$ (again, the justification of the factor being exactly 2 really needing a fuller analysis). From Kirkhoff's laws and the Josephson relation we have

$$2\pi=\int \frac{d\phi}{dt}dt=\frac{2e}{\hbar}\int Vdt=\frac{2e}{\hbar}R_s\int Idt=\frac{2e}{\hbar}\Delta q. \tag{35}$$

Here Δq is the amount of charge that passes through the shunt resistor as a result of the QPS. In units of the charge of a Cooper pair, $2e$, this is

$$\frac{\Delta q}{2e}=\frac{R_Q}{R_S}. \tag{36}$$

We thus guess that the normal state is stable when $R_S>R_Q$. The basic physics is that fluctuating QPS's act as voltage noise that gives rise to charge fluctuations on the junction. The insulating state is only stable when these charge fluctuations are sufficiently small: less than $2e$.

The generalization of the single-junction argument to the system in Fig. 2 requires analysis of the effective shunting resistances for the various QPS configurations. The quantum phase slips are effectively voltage sources. The phase slip dipole corresponding to ζ_- is thus equivalent to two equal but opposite voltage sources across the two junctions so that there is no voltage between the two leads, but the grain is at a different voltage than the leads.

(i) The FSC-to-N1-S2 transition is determined by the circuit in Fig. 8(a). In this case junction two can be replaced by a short as it is superconducting on both sides of the transition. This gives an effective shunting resistance $R_1+rR_2/(R_2+r)$ for the phase slip, so the transition occurs at $R_1+rR_2/(R_2+r)=R_Q$. Similarly, the transition between

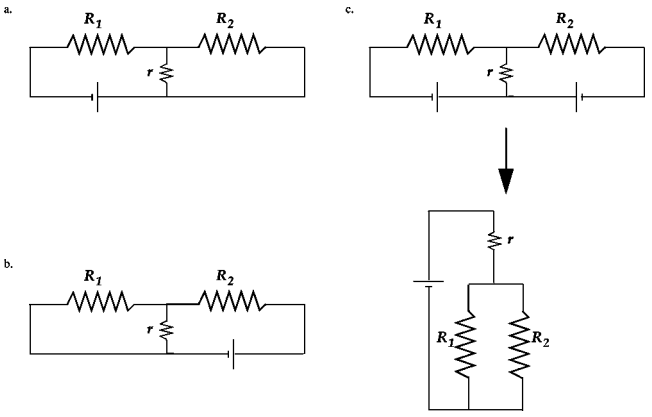

FIG. 8. Effective circuits for transitions to the FSC phase in the phase-slip picture. Phase slips correspond to a voltage source across the corresponding junction. (a) Phase slip on junction 1, (b) phase slip on junction 2, and (c) slip-antislip pair which corresponds to slipping the phase of the grain relative to both leads.

S1-N2 and FSC is determined by the circuit in Fig. 8(b), with the effective shunting resistance at the transition being $R_2 + rR_1/(R_1+r) = R_Q$.

(ii) To understand the FSC-to-SC* transition we need to consider a dipole consisting of a QPS on junction 1 and a simultaneous anti-QPS on junction 2, corresponding to a 2π phase twist on the intervening grain. In particular, we need to know how much charge flows from the super electrons on the grain to the normal electrons on the grain during such a phase twist. An equivalent circuit is shown in Fig. 8(c), and we conclude that the phase boundary should occur at $r + R_1R_2/(R_1+R_2) = R_Q$, as the charge must flow through r and either R_1 or R_2.

(iii) The transition between S1-N2 and the NOR phase is determined by the relevance of the QPS on junction 1 when junction 2 is insulating. The corresponding circuit is shown in Fig. 9(a); since the effective shunting resistance is $R_1 + r$, we find a phase boundary at $R_1 + r = R_Q$. Similarly, the N1-S2-to-NOR transition is at $R_2 + r = R_Q$.

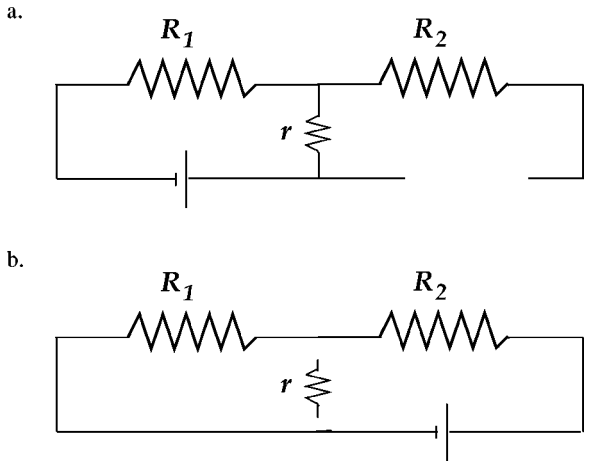

FIG. 9. Effective circuits for transitions to the NOR phase in the phase-slip picture. (a) Phase slip on junction 1 when junction 2 is insulating (ζ_2 is relevant) and (b) phase slip on junction 1 (or 2) when ζ_- is relevant and slip-antislip pairs proliferate.

(iv) The transition between SC* and NOR is determined by the effective circuit in Fig. 9(b). In the SC* phase the component that is incoherent with the rest of the system is the grain. Since phase coherence between the leads is maintained, charge can flow freely from lead to lead via virtual superconducting electrons on the grain unhindered by the phase fluctuations on the grain. But if some charge flows through r to the normal electrons on the grain, this current will couple to the phase-slip dipoles and induce a large voltage drop; hence r becomes effectively a disconnect in the SC* phase. The destruction of lead-to-lead superconductivity that characterizes the SC*-to-NOR transition thus occurs at $R_1 + R_2 = R_Q$.

(v) The FSC-to-NOR line is naively a continuation of the S1-N2 and N1-S2 lines. This suggests that to approach the transition line from the superconducting side, when we consider a QPS in junction 1 we assume junction 2 to be superconducting and vice versa. This highly questionable approximation reflects the limitations of our strong-coupling analysis for the FSC-to-NOR transition; we will analyze it more carefully below.

V. INTERMEDIATE-COUPLING FIXED POINT

In the previous two sections we have analyzed the zero-temperature states and transitions between them in both the weak- and strong-Josephson-coupling limits. In both cases, we found that there were some regimes that could not be adequately analyzed. In this section analyze the intermediate-coupling behavior, finding that transitions occur whose locations and properties are not given correctly by either the weak- or strong-coupling approaches.

A comparison of Fig. 4 and Fig. 7 reveals that there is a difference between weak- and strong-coupling phase diagrams for $r < R_Q$. In particular, the inferred phase boundaries between the FSC and NOR phases differ in these two limits. This transition is special in that *both* junctions go from superconducting to normal, but the transition is driven by the dynamics of just one of them. In the weak-coupling limit, when we analyzed the superconductor-to-normal transition of junction 1, our underlying assumption was that junction 2 was normal. By contrast, for the same transition in the strong-coupling case, junction 2 was assumed to be effectively superconducting. This distinction between the approximate descriptions accounts for the difference in inferred phase diagrams. What is the actual behavior in this regime? Does it, in contrast to the other regimes, depend on the magnitudes of the Josephson couplings as well as the resistances?

In Fig. 10 we indicate parts of the phase diagram for which weak- and strong-coupling analyses suggest different natures of the ground state. These regimes of the resistances would be fully superconducting (FSC) in the strong-coupling approximation and normal (NOR) in the weak-coupling approximation: the FSC fixed manifold is stable to small fugacities of the phase slips, and the NOR fixed manifold is stable to small Josephson couplings. This suggests that in such regimes, there should be a transition from NOR to FSC as the J's are varied at a finite nonzero value of the Josephson couplings. Specifically, if an appropriate combination of

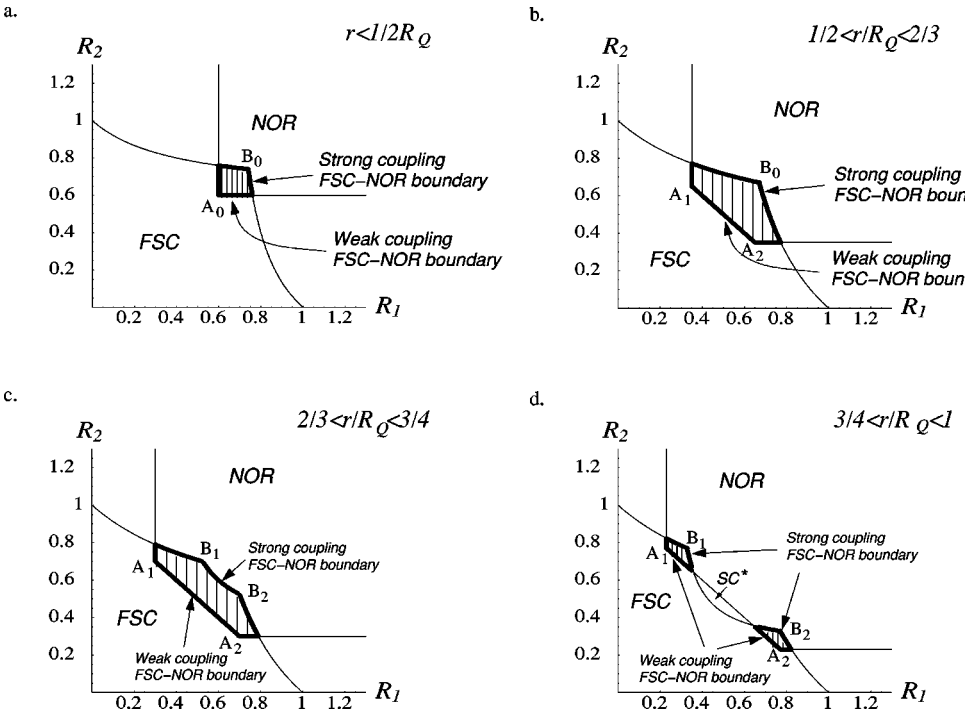

FIG. 10. Intermediate-coupling fixed-point regions of the phase diagram. The shaded regions surrounded by a bold line lie in a superconducting phase for strong coupling and in an insulating phase for weak coupling. For $r>R_Q$ there are no such regions. For intermediate J the phase boundaries will be in the shaded regions. The points A_0, A_1, and A_2 mark where the critical fixed point, J^* goes to zero, and the points B_0,B_1, and B_2 mark where ζ^* goes to zero corresponding to $J^*\to\infty$. Near these multicritical points the RG analyses in the text become exact.

the Josephson couplings is greater than some (resistance dependent) critical value, then the system will be in the FSC state, while if this combination is less than the critical value, the system will be in the normal state. As such a transition is presumably controlled by an intermediate-coupling fixed point, it will have very different character than the other transitions; from now on we will refer to regimes in which such critical fixed points occur as simply *intermediate* regimes.

It is useful to remember that the original microscopic model had $J_+=0$, so for fixed resistances in the intermediate regime, on the J_1,J_2 plane there will be a manifold below which the system flows to the normal fixed point and above which it flows to the FSC fixed point; this is the critical manifold of the FSC-to-NOR transition. Alternatively, the microscopic model could be defined in terms of the phase-slip fugacities ζ_1,ζ_2 with $\zeta_-=0$. For fixed resistances in the intermediate regime, the critical manifold would show up here too, separating the FSC and normal phases in, for fixed resistances, the ζ_1,ζ_2 plane.

In general, an analysis of the critical behavior in the intermediate regime is beyond the methods of this paper, but we can make use of the weak- and strong-coupling limits to analyze *parts* of this regime: specifically, when the critical values of either the Josephson couplings or the QPS fugacities, respectively, are small.

A. Weak-coupling limit

We first study the weak-coupling limit. In order to find the critical values of J_1,J_2,J_+ in the intermediate regime, we need to analyze the effects of the nonlinear terms in the RG flow equations (27) and, if there is indeed a perturbatively accessible critical fixed point, find it and the corresponding critical manifold. Truncating at second order, we indeed find a fixed point

$$(J_1^*)^2=\frac{(R_2+r-R_Q)(R_1+R_2-R_Q)}{rR_1},$$

$$(J_2^*)^2=\frac{(R_1+r-R_Q)(R_1+R_2-R_Q)}{rR_2},$$

$$(J_+^*)^2=\frac{(R_2+r-R_Q)(R_1+r-r_Q)}{R_2R_1}, \tag{37}$$

with an overall cutoff-dependent proportionality coefficient having been set equal to unity when the RG equations were first derived. As we see below, this fixed point can be shown to be critical provided each of the three resistance combinations in parentheses are positive. These factors, which we will call

$$u\equiv R_2+r-R_Q,\quad v\equiv R_1+r-R_Q,\quad w\equiv R_1+R_2-R_Q, \tag{38}$$

are the negatives of the eigenvalues of the three couplings along the normal fixed manifold so that the normal phase is stable to small J's in this regime as indicated by the weak-coupling phase diagram. Naively, one might have expected the nonlinear perturbative analysis to be valid only when all three of these eigenvalues are small, but we see that in fact all that is needed is *two of the three eigenvalues small and negative* with the third being arbitrarily negative. Correspondingly, we require that all three of u, v, and w be positive with two of them being small.

By rescaling the J's appropriately, the RG flows can be put in a simple symmetric form in terms of u, v, and w, and the fixed point values written as

$$J_1^*=\sqrt{\frac{uw}{rR_1}},\quad J_2^*=\sqrt{\frac{vw}{rR_2}},\quad J_+^*=\sqrt{\frac{uv}{R_1R_2}}. \tag{39}$$

The linearized flows around this intermediate-coupling fixed point yield the eigenvalues which are given by

$$\lambda_i \approx \Lambda_i (u+v+w), \tag{40}$$

with the $\{\Lambda_i\}$ being the three roots of

$$\Lambda^3 + \Lambda^2 = m \tag{41}$$

in terms of the dimensionless combination of the resistances

$$m \equiv \frac{4uvw}{(u+v+w)^3}. \tag{42}$$

We see immediately that for m positive, as it must be, there is always a unique positive eigenvalue λ_+, which controls the growth of deviations from the critical manifold; the two others have negative real parts and are hence irrelevant at the intermediate-coupling critical fixed point. Note that if only two of u, v, and w are small, with, say, w being much larger than the other two, then $\Lambda_+ \approx \sqrt{4uv/w^2} \ll 1$ so that $\lambda_+ \approx 2\sqrt{uv}$. If all three are small and comparable, λ_+ will be of the same order but depend in a somewhat complicated way on their ratios.

B. Strong-coupling limit

It is clear by examining the limits of validity of the weak-coupling expansion above that we cannot extract the critical behavior throughout the intermediate regime from this analysis. Fortunately, we can access another part of this regime from the strong-coupling direction.

Using the second-order RG flows in terms of the fugacities of phase slips, we find a critical fixed point at

$$(\zeta_1^*)^2 = \left(\frac{1}{R_Q} - \frac{R_2+R_1}{Y}\right)\left(\frac{1}{R_Q} - \frac{r+R_1}{Y}\right)\frac{Q^2}{rR_2},$$

$$(\zeta_2^*)^2 = \left(\frac{1}{R_Q} - \frac{R_2+R_1}{Y}\right)\left(\frac{1}{R_Q} - \frac{r+R_2}{Y}\right)\frac{Q^2}{rR_1},$$

$$(\zeta_-^*)^2 = \left(\frac{1}{R_Q} - \frac{R_2+r}{Y}\right)\left(\frac{1}{R_Q} - \frac{r+R_1}{Y}\right)\frac{Q^2}{R_1R_2}, \tag{43}$$

with $Y = r(R_1+R_2)+R_1R_2$. As for weak coupling, it is convenient to work in terms of the negatives of the eigenvalues of the three fugacities about the FSC fixed manifold, defining

$$\underline{u} \equiv \frac{R_2+r}{Y} - R_Q,$$

$$\underline{v} \equiv \frac{R_1+r}{Y} - R_Q,$$

$$\underline{w} \equiv \frac{R_1+R_2}{Y} - R_Q, \tag{44}$$

with the condition for the validity of the expansion being that all these must be positive with at least two of them small. The expansion is carried out in exactly the same manner as for the weak-coupling limit and the eigenvalues about the intermediate-coupling critical fixed point determined by exactly the same conditions as in Eqs. (40)–(42), with simply u, v, and w replaced by their (overbared) strong-coupling equivalents.

C. Superconducting-normal critical manifold

From the above discussion we see that direct transitions between the FSC and NOR phases will always be controlled by intermediate-coupling fixed points. Although we thus cannot find the full phase boundary exactly in the intermediate region of the resistance space, we can use the weak- and strong-coupling analysis to find it in some regimes of the intermediate region. Equations (37) and (43) apply in the weak- and strong-Josephson-coupling limits, respectively, so that we can locate the phase boundaries accurately in the intermediate region from the flow equations provided that both the bare and fixed-point values of the Josephson couplings are either all large or all small. In particular, we have found that the J^* go to zero along certain lines in the r, R_1, and R_2 space which intersect the constant r surfaces shown in Fig. 10 at the points A_0, A_1, and A_2; our weak-coupling analysis is controlled in their vicinity providing the bare J's are small. Analogously, the fixed-point values ζ_i^* vanish at points B_0, B_1, and B_2 of the constant-r surfaces as shown in Fig. 10 and the strong-coupling analysis is controlled in their vicinity provided the bare J's are large.

The finite values of the J^*'s at the fixed point on the critical lines have interesting implications for the phase boundaries in the full R and J parameter space as sketched in Fig. 11. If we cross from the FSC to NOR phase by changing resistances and keeping J's fixed, the exact location of the transition will generally depend on the values of the J's. However, there is a whole range of small J's (which we can schematically denote as $0<J<J^*$) for which, in the second-order RG approximation, this transition occurs exactly at the FSC-to-intermediate-region boundary; if we consider higher-order terms in the RG, the location of the transition in this range will be modified slightly. Analogously there is a range of large J's for which the FSC-to-NOR transition happens very close to the intermediate-region-to-NOR line (in strong coupling this occurs for $0<\zeta<\zeta^*$).

For illustrative purposes we calculate explicitly the phase boundary as a function of weak $J_{1,2}$ in the part of the intermediate regime of resistances in which the fixed point is at small but nonzero coupling. In particular, we consider the FSC-to-NOR transition for

$$r<0.5, \quad R_2 = 1-r+u, \quad R_1 = 1-r+v, \tag{45}$$

with u and v small, and for convenience, we set $R_Q=1$ for this section. The third parameter

$$w = R_1+R_2-1 = 1-2r+u+v \approx 1-2r \tag{46}$$

is generally *not* small. It is convenient to define rescaled couplings by

$$K_1 \equiv \sqrt{\frac{r(1-r)}{1-2r}}J_1, \quad K_2 \equiv \sqrt{\frac{r(1-r)}{1-2r}}J_2, \tag{47}$$

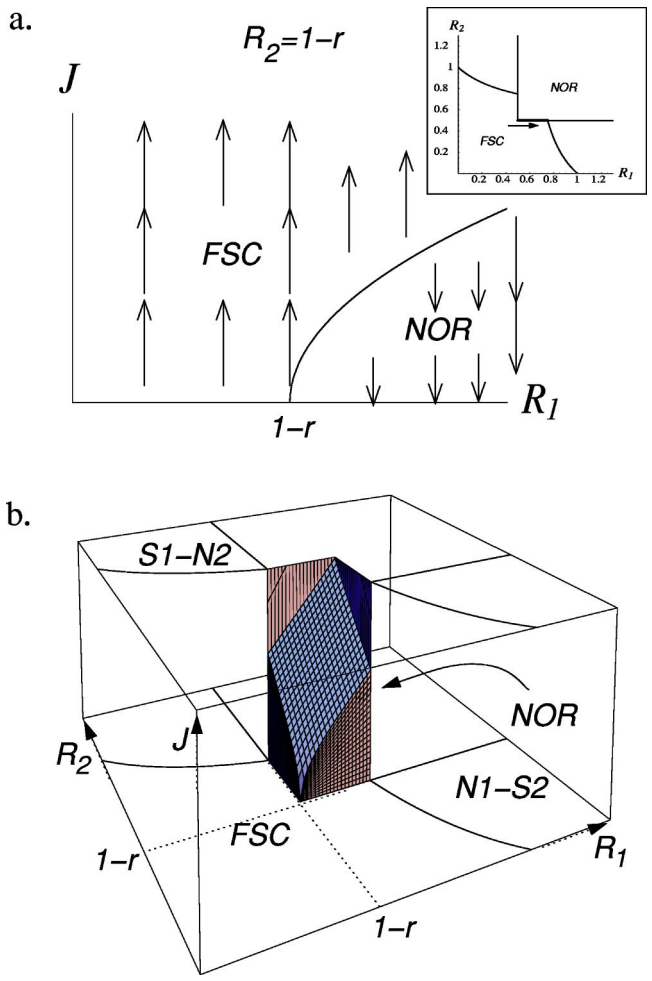

FIG. 11. Example of phase diagram in vicinity of a transition between the FSC and NOR phases for fixed $r<1/2$. The critical manifold in the intermediate regime depends on the Josephson coupling strengths. (a) Schematic cross section of the phase diagram along the line with $R_2=1-r$ (this line is the bold line indicated by an arrow in the inset) showing the jump in J_c suggested by the truncated second-order RG analysis for crossing the phase boundary from $R_2<1-r$ to $R_2>1-r$. The arrows indicate the RG flow of the Josephson couplings. Higher-order terms in RG flows are likely to drive the critical J_c to zero on the line $R_2=1-r$. (b) Three-dimensional view of the phase diagram, focusing on the FSC-NOR transition. The solid lines in the *x*-*y* plane mark the phase boundary between the mixed phases and the insulating and the FSC phases. These phase boundaries are independent of J.

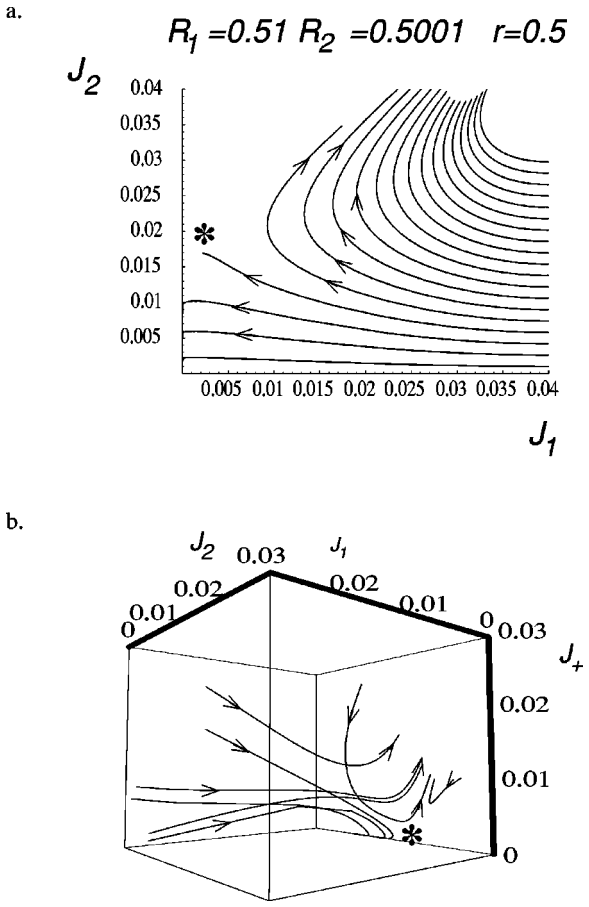

FIG. 12. RG flows in the intermediate region with $R_1=0.51$, $R_2=0.5001$, and $r=0.5$. Note the typical flow pattern in the vicinity of the unstable critical fixed point marked by an asterisk. (a) Projection of the RG flow trajectories on the J_1,J_2 plane. (b) A 3D flow diagram for near-critical trajectories.

which have fixed-point values $K_1^*\approx\sqrt{u}$ and $K_2^*\approx\sqrt{v}$. From the RG flow equations, it can be seen that J_+ rapidly approaches its nullcline value $J_+^n(K_1,K_2)$ and then evolves slowly with the other variables. Substituting J_+^n for J_+ in the flow equations for $K_{1,2}$, we can find the invariant manifold on which the critical fixed point lies. This is parametrized by

$$K_1^2-u[1+\ln(K_1^2/u)]\approx K_2^2-v[1+\ln(K_2^2/v)], \qquad (48)$$

which has two branches of solutions: the branch with one of K_1 or K_2 larger than its fixed-point value and the other smaller is the desired critical manifold. Note that as J_1 increases above its fixed-point value, the critical value of J_2 decreases exponentially and vice versa. Although we have taken the bare $J_+=0$, even a J_+ of the order of the fixed-point values of the other J's will not appreciably change their critical values in this regime with $w\gg u,v$.

A similar analysis can be done with either of the other pairs u, w or v, w both small and the third of order unity. In these cases, however, the smallness of the bare J_+ means that the early stages of the renormalization will give rise to a nonzero value of J_+ at intermediate scales whose value is needed to estimate the critical condition that relates the other J's. An example of the RG flow of the J's near the boundary of the intermediate coupling region is shown in Fig. 12.

Symmetric case. Although unrealistic for the physical model of two junctions, it is instructive to consider the case in which there is a symmetry between the three superconducting components and the Josephson couplings linking them. In this case we take

$$r=R_1=R_2=R \quad \text{and} \quad J_+=J_1=J_2=J, \qquad (49)$$

and the RG flow equations become simply

$$\frac{dJ}{d\ell}\approx J(1-2R)+RJ^2, \qquad (50)$$

with

$$w = u = v = 2R - 1, \tag{51}$$

so that the weak-coupling part of the intermediate region occurs for R slightly bigger than $\frac{1}{2}R_Q$. The critical value of J is then simply

$$J_c \approx J^* \approx 4\left(R - \frac{1}{2}\right), \tag{52}$$

and the RG eigenvalue controlling flows away from this is

$$\lambda \approx 2\left(R - \frac{1}{2}\right). \tag{53}$$

In the strong-coupling limit, we can similarly use a single QPS fugacity ζ and write

$$\frac{d\zeta}{d\ell} \approx \zeta\left(1 - \frac{2}{3R}\right) + \frac{1}{R}\zeta^2, \tag{54}$$

so that the intermediate region occurs for

$$\frac{1}{2} < R < \frac{2}{3}. \tag{55}$$

Near the upper end of this range, R is slightly less than $\frac{2}{3}$, the critical value of the fugacity is small, and the RG eigenvalue for deviations from criticality becomes

$$\lambda \approx \frac{3}{2}\left(\frac{2}{3} - R\right). \tag{56}$$

Comparing the two limiting expressions for λ, we see that, for the symmetric case, it is unlikely to get above a small value of order 0.2 anywhere in the intermediate region.

VI. SYMMETRIES OF THE TWO-JUNCTION SYSTEM

From the microscopic model of Fig. 2, the only obvious symmetry—more properly a simple duality—is the exchange of the two junctions, $R_1 \leftrightarrow R_2$ and $J_1 \leftrightarrow J_2$. The analysis presented in this section uncovers additional symmetries in the phase diagram of the system at zero temperature; indeed, in the analysis of the previous section we have already seen evidence of these. Here we will show more generally that the junction interchange is only one part of a larger permutation symmetry, or triality, that involves the interchange of all resistors r, R_1, and R_2 and the corresponding Josephson couplings. We also show how the familiar weak- to strong-coupling duality of a single shunted Josephson junction[43,67] can be generalized to the two-junction system. These symmetries allow one to relate in a nontrivial way many of the phase boundaries shown in Fig. 10.

A. Permutation triality

The two-junction system exhibits three normal phases and two superconducting ones. The simplest insulating phase involves proliferations of all three kinds of phase slips. Conversely, the simplest superconducting phase, the fully superconducting one, FSC, has none of the phase slips proliferating. Of the three remaining phases, two are normal as far as interlead properties are concerned, because of phase slips that proliferate in *one* of the two junctions. The last phase is the SC* phase, which is superconducting because it exhibits dissipationless lead-to-lead transport due to Cooper-pair cotunneling processes. This phase, however, also has signatures of normal phases, in particular localized charges on the middle grain and the proliferation of QPS–anti-QPS pairs that decouple the phase of this grain from the linked superconductivity of the two leads.

An alternative way to group the five phases is thus as one purely normal phase, one purely superconducting phase, and three mixed phases, in which part of the system is normal and part is superconducting. In terms of phase-slip fugacities, these correspond, respectively, to one phase in which all fugacities grow under the RG transformation, one phase in which all fugacities renormalize to zero, and three phases in which only one of the fugacities ζ_1, ζ_2, and ζ_- grows under RG, while the remaining two renormalize to zero. Such grouping is very suggestive of a permutation symmetry of the full phase diagram in which the phases N1-S2, S1-N2, and SC* are transformed into each other, and phases FSC and NOR are invariant. In this section we show that such triality is indeed present in the low-energy properties of the microscopic models (23) and (32) describing the system. Note that other systems possessing triality have been discussed earlier Shankar in Ref. 68; as in our case, these are nontrivial in some representations but easy to see in others.

To demonstrate the triality in the original quantum action we consider the strong coupling representation of Eq. (32), although equivalent arguments can be made for the weak-coupling representation described by Eq. (23). Let us begin with the mathematical formulation of this symmetry.

The action in Eq. (32) reads

$$Z = \int D[\theta_1] \int D[\theta_2] \exp\Bigg(-\beta \sum_{\omega_n} |\omega_n| \vec{\theta}^T_{-\omega_n} \hat{R} \vec{\theta}_{\omega_n} + \int_0^\beta d\tau [\zeta_1 \cos(\theta_1) + \zeta_2 \cos(\theta_2) + \zeta_- \cos(\theta_1 - \theta_2)] \Bigg), \tag{57}$$

where the resistance matrix is

$$\hat{R} = \begin{pmatrix} r + R_1 & -r \\ -r & r + R_2 \end{pmatrix}, \tag{58}$$

and the vector $\vec{\theta}$ has components $\theta_{1,2}$. An interchange of the two junctions, $R_1 \leftrightarrow R_2$ and $\zeta_1 \leftrightarrow \zeta_2$, will leave the phase diagram invariant, exchanging the two mixed states in which one junction is superconducting and the other is normal (N1-S2 and S1-N2). In Eq. (58) this interchange of junctions corresponds to transforming the fields, $\theta_1 \leftrightarrow \theta_2$, or

$$\begin{pmatrix} \theta_1 \\ \theta_2 \end{pmatrix} = \begin{pmatrix} 0 & 1 \\ 1 & 0 \end{pmatrix} \begin{pmatrix} \theta_1' \\ \theta_2' \end{pmatrix}. \tag{59}$$

In terms of the new variables $\vec{\theta}' = \hat{S}^{-1}\vec{\theta}$,

$$Z=\int D[\theta_1']\int D[\theta_2']\exp\Bigg(-\beta\sum_{\omega_n}|\omega_n|\vec{\theta}'^{\,T}_{-\omega_n}\hat{R}'\vec{\theta}'_{\omega_n} + \int_0^\beta d\tau[\zeta_1\cos(\theta_1')+\zeta_2\cos(\theta_2')+\zeta_-\cos(\theta_1'-\theta_2')]\Bigg), \tag{60}$$

where

$$\hat{R}'=\hat{S}^T\hat{R}\hat{S}=\begin{pmatrix} r+R_2 & -r \\ -r & r+R_1\end{pmatrix},$$

$$\zeta_1'=\zeta_2 \quad \zeta_2'=\zeta_1 \quad \zeta_-'=\zeta_- . \tag{61}$$

This new action (60) and (61) has $R_1\leftrightarrow R_2$ and $\zeta_1\leftrightarrow\zeta_2$ but otherwise exactly the same physics with simply relabeling the fields θ_i.

A less trivial symmetry involves the transformation

$$\begin{pmatrix}\theta_1\\ \theta_2\end{pmatrix}=\begin{pmatrix}1 & 0\\ 1 & -1\end{pmatrix}\begin{pmatrix}\theta_1'\\ \theta_2'\end{pmatrix}, \tag{62}$$

leading to the action (60) with

$$\hat{R}'=\begin{pmatrix} R_1+R_2 & -R_2 \\ -R_2 & r+R_2\end{pmatrix},$$

$$\zeta_1'=\zeta_1 \quad \zeta_2'=\zeta_- \quad \zeta_-'=\zeta_2 . \tag{63}$$

This new symmetry is surprising as it swaps R_2 with r. One way of understanding this is as a change of basis for the quantum phase slips. Earlier we took QPS's on junctions 1 and 2 as a basis [schematically, we can label them as $(1,0)$ and $(0,1)$] and considered a QPS dipole as their composite: $(1,-1)=(1,0)+(0,-1)$. An equivalent basis set, however, can be obtained by taking one of the QPS's and the dipole as the basic objects, and viewing the other QPS's as their composite—e.g., $(0,1)=(1,0)+(-1,1)$. The corresponding transformation (62) maps phases S1-N2 and SC* into each other, while leaving the other ones intact.

Using transformations (59) and (62) one can construct transformations that permute *any* of the three resistances and connect any of the phases N1-S2, S1-N2, and SC*. The physical basis of this symmetry follows from the observation that the circuits corresponding to the three kinds of phase slips are similar; one resistor is connected in series to the two other resistors, which are connected in parallel. (The strong-coupling representation we are using here implies starting from the FSC phase as in Sec. IV C). From the circuit diagrams in Fig. 8 we see the origin of the permutation symmetry: circuits associated with all three kinds of phase slips differ only in the exchange of resistors. The strong-coupling permutation triality thus generally corresponds to

$$\zeta_i'=\zeta_{\pi_{(i)}},$$

$$R_i=R_{\pi_{(i)}}, \tag{64}$$

with $i=1,2,-$, where we have paired the fugacities with the corresponding resistance, so that $R_+=r$ and π is a permutation of the three indices.

In the weak-coupling regime, the nature of the triality is the same: the circuits corresponding to the three Cooper-pair tunneling events are similar with two resistors in series and a third taken out of the circuit. (Use of the weak-coupling representation implies starting from the NOR phase; see Sec. III C.) If we now pair the Josephson couplings with the corresponding missing resistor in the equivalent circuits, $r_1=R_2, r_2=R_1$, and $r_+=r$, the permutation symmetry in the weak-coupling limit becomes

$$J_i'=J_{\pi_{(i)}},$$

$$r_i'=r_{\pi_{(i)}}, \tag{65}$$

with $i=1,2,+$, where π is again a permutation.

B. Weak- to strong-coupling duality

The similar form of the strong-coupling and weak-coupling representations of the quantum actions (23) and (32) suggests that there is a duality between the two regimes.

The duality we find is a generalization of that of a single resistively shunted Josephson junction (see, e.g., Ref. 69). For the single junction the duality is equivalent to the observation that quantum phase slips in a junction with shunt resistance R behave similarly, as far as their quantum statistical mechanics, to Cooper-pair tunneling events in a junction with shunt resistance $\tilde{R}=R_Q^2/R$. In the two-junction problem discussed in this paper we expect that Cooper-pair tunneling events across any of the junctions in weak coupling should be dual to quantum phase slips on the same junction in strong coupling, and Cooper pair cotunneling processes across the two junctions should be dual to QPS dipoles on the two junctions. But a complication is that the effective resistance for a Cooper-pair tunneling event (or a QPS) in one of the junctions depends on the state of the other junction (see Secs. III C and IV C).

The duality transformation maps Cooper pairs into QPS's and superconducting phases into normal ones. Hence, when we discuss the duality between Cooper tunneling events and QPS's on any given junction, we need the duality transformation to change the *state* of the other junction. For example, consider a Cooper-pair tunneling through junction 1 with junction 2 normal. The dual of this will be a QPS on junction 1, with junction 2 superconducting. Comparison of the effective shunting resistances in the two cases immediately gives the duality relation

$$\tilde{R}_1+\tilde{r}=\frac{R_Q^2}{R_1+\dfrac{rR_2}{r+R_2}}. \tag{66}$$

Analogous arguments give

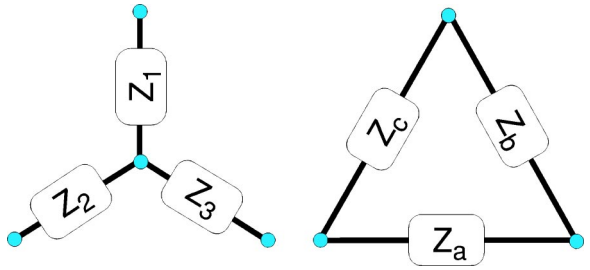

FIG. 13. $Y\leftrightarrow\Delta$ transformation. "Y" resistor network on left is mapped to Δ network on right via $Z_1Z_a=Z_2Z_b=Z_3Z_c=Z_1Z_2+Z_2Z_3+Z_3Z_1$. The inverse transformation ($\Delta\rightarrow$Y) is $Z_bZ_c/Z_1=Z_cZ_a/Z_2=Z_aZ_b/Z_3=Z_a+Z_b+Z_c$.

$$\tilde{R}_2+\tilde{r}=\frac{R_Q^2}{R_2+\dfrac{rR_1}{r+R_1}},$$

$$\tilde{R}_1+R_2'=\frac{R_Q^2}{r+\dfrac{R_1R_2}{R_1+R_2}}. \tag{67}$$

An alternative way of seeing the duality is to take $\theta_1\rightarrow\Delta_1'$ and $\theta_2\rightarrow-\Delta_2'$ in action (32). The cosine terms of the resulting action in terms of (Δ_1',Δ_2') and those of the weak-coupling action (23) then have the same form. If we compare the quadratic terms in these actions, we find the same duality relations (66) and (67).

We can solve the duality relations (66) and (67) for $\tilde{r},\tilde{R}_1$, and $\tilde{R}_2$:

$$\tilde{r}=R_Q^2\frac{r}{Y},$$

$$\tilde{R}_1=R_Q^2\frac{R_2}{Y},$$

$$\tilde{R}_2=R_Q^2\frac{R_1}{Y}, \tag{68}$$

with $Y\equiv rR_1+rR_2+R_1R_2$. This mapping of the resistors to dual resistors may seem rather unintuitive; however, Eqs. (68) coincides with the well-known "Y-Δ" transformation of resistor networks. The Y-Δ transformation is depicted in Fig. 13. By comparing the Y-Δ transformation equations in Fig. 13 we see that the duality transforms the system in Fig. 14(a) to the system in Fig. 14(b). In Fig. 14(a) the resistors R_1,R_2, and r are connected in a "Y" pattern; the transformed system has the resistances $R_Q^2/R_2,R_Q^2/R_1$, and R_Q^2/r connected a Δ pattern.

This statement of the duality is simple; pair-tunneling events (current sources) with a Y resistance network and resistors r,R_1, and R_2 [Fig. 14(a)] are dual to quantum phase slips (voltage sources) with a Δ network of resistances $R_Q^2/r,R_Q^2/R_1$, and R_Q^2/R_2 [Fig. 14(b)]. This is a simple generalization of the single junction duality. From Fig. 14 we see that as $r\rightarrow0$ the duality reduces to

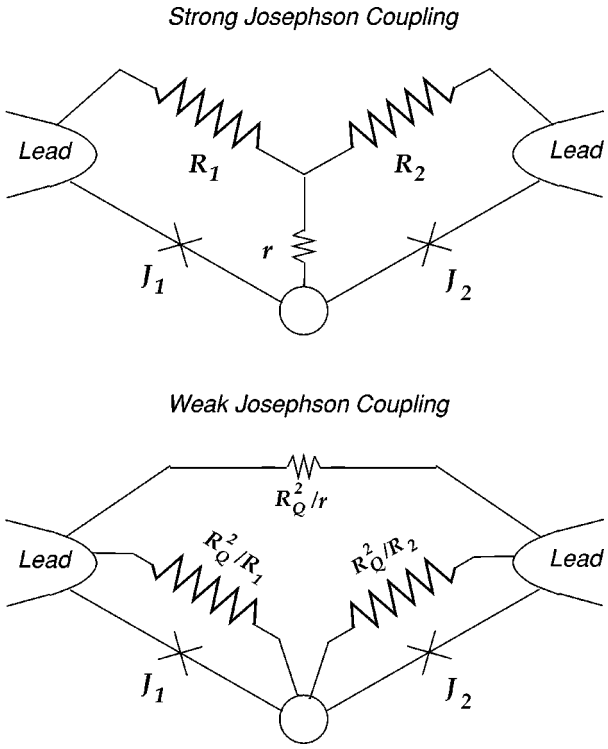

FIG. 14. (a) Original circuit of Fig. 2 in the weak-coupling limit showing a "Y" resistor network. (b) Strong-coupling dual of the circuit showing a "Δ" shaped network. The network in (b) captures the duality, Eqs. (68).

$$\tilde{r}=0,$$

$$\tilde{R}_1=\frac{R_Q^2}{R_1},$$

$$\tilde{R}_2=\frac{R_Q^2}{R_2},$$

which is simply the duality of a single junction applied to the two uncoupled junctions, as should be expected in this limit in which the middle grain is macroscopic.

C. Phase boundaries controlled by weak or strong coupling

The weak-to-strong coupling duality yields a mapping between several of the phase boundaries in Fig. 10 onto each other. The nature of this mapping is such that weak-coupling transitions will be mapped to strong-coupling ones; e.g., the NOR-to-N1-S2 boundary gets mapped into the FSC-to-S1-N2 boundary. Here NOR to N1-S2 corresponds to a weak-coupling transition, since it involves ordering of Δ_2 with Δ_1 remaining disordered on both sides of the transition; i.e., J_2 becomes relevant, while J_1 and J_+ stay irrelevant. By contrast S1-N2 to FSC is really a strong-coupling transition because it involves J_2 becoming relevant with J_1 already relevant. This latter transition is simple in terms of the QPS fugacities, corresponding to ζ_2 becoming relevant about the FSC manifold with ζ_1 and ζ_- irrelevant on both sides of the phase boundary.

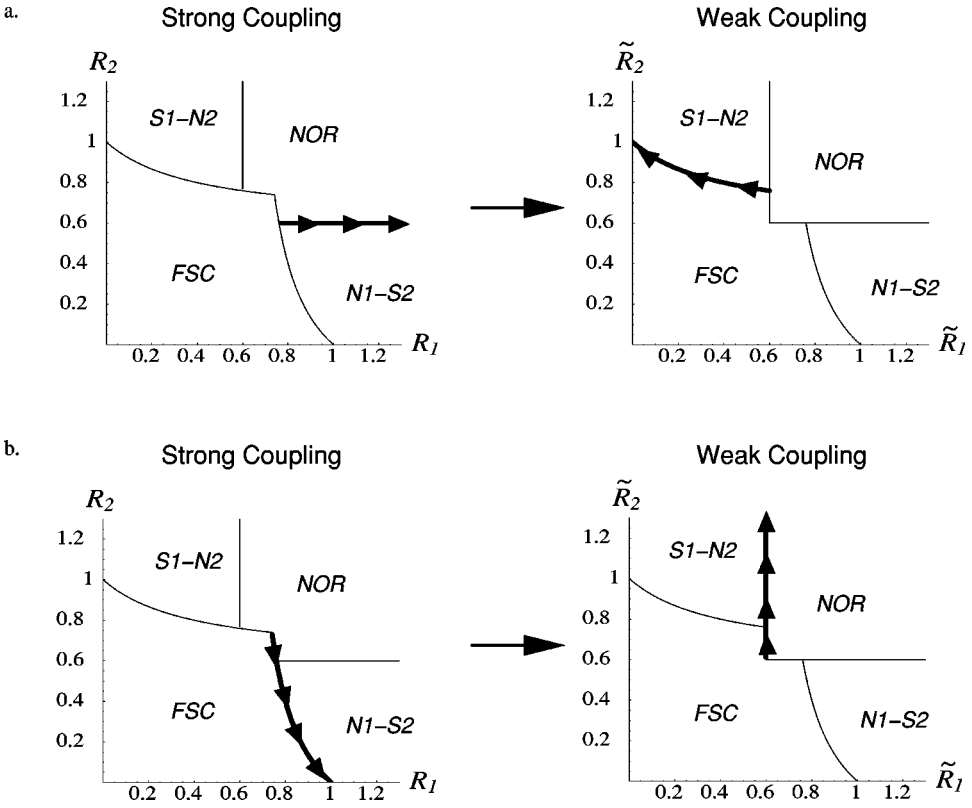

FIG. 15. Weak-strong duality: (a) mapping of the strong-coupling critical line $R_2+r=1$ to the weak-coupling regime and (b) mapping of the strong-coupling critical line $R_1+R_2r/(R_2+r)=1$ to the weak-coupling regime.

First, we map the phase boundary $R_2+r=R_Q$ via Eqs. (68). After substituting $r=R_Q-R_2$ this yields

$$\tilde{r}=\frac{R_Q^2}{R_1+R_2+\dfrac{R_1R_2}{R_Q-R_2}}=R_Q\frac{R_Q-R_2}{R_1+R_2-R_2^2/R_Q},$$

$$\tilde{R}_1=\frac{R_Q^2}{R_Q+R_1-R_2+\dfrac{R_1(R_Q-R_2)}{R_2}}=R_Q\frac{R_2}{R_1+R_2-R_2^2/R_Q},$$

$$\tilde{R}_2=\frac{R_Q^2}{R_Q+\dfrac{R_2(R_Q-R_2)}{R_1}}=R_Q\frac{R_1}{R_1+R_2-R_2^2/R_Q}. \quad (69)$$

These apparently complicated expressions are simply the boundary of the FSC phase, since

$$\frac{1+\dfrac{\tilde{R}_1}{\tilde{r}}}{\tilde{R}_1+\tilde{R}_2+\dfrac{\tilde{R}_1\tilde{R}_2}{\tilde{r}}}=\frac{1}{\tilde{R}_2+\dfrac{\tilde{r}\tilde{R}_1}{\tilde{r}+\tilde{R}_1}}$$

$$=\frac{1}{R_Q}\frac{R_1+R_2-R_2^2/R_Q}{R_1+(R_Q-R_2)R_2/R_Q}=\frac{1}{R_Q}, \quad (70)$$

as shown in Fig. 15(a). As a second example, consider the critical line $R_1+R_2r/(R_2+r)=1$, which separates the FSC phase from the mixed phase in which junction 1 is normal. The duality equations yield

$$\tilde{r}=\frac{R_Q^2}{R_1+R_2+\dfrac{R_1R_2(R_1+R_2-R_Q)}{R_2(R_Q-R_1)}}=R_Q\frac{R_Q-R_1}{R_2},$$

$$\tilde{R}_1=\frac{R_Q^2}{R_1+\dfrac{R_2(R_Q-R_1)}{R_1+R_2-R_Q}+\dfrac{R_1R_2(R_Q-R_1)}{(R_2+R_1-R_Q)R_2}}$$

$$=R_Q\frac{R_1+R_2-R_Q}{R_2},$$

$$\tilde{R}_2=\frac{R_Q^2}{R_2+\dfrac{R_2(R_Q-R_1)}{R_1+R_2-R_Q}+\dfrac{R_2^2(R_Q-R_1)}{(R_2+R_1-R_Q)R_1}}$$

$$=R_Q\frac{R_1(R_1+R_2-R_Q)}{R_2^2}, \quad (71)$$

so that

$$\tilde{R}_1+\tilde{r}=R_Q, \quad (72)$$

which is the condition for the phase boundary between the normal phase and the mixed phase in which junction 1 is superconducting, as in Fig. 15(b).

D. Duality in the intermediate region

In the intermediate regime of the resistance parameter space, the behavior under duality is more complicated. Since the controlling critical fixed point that determines the fully normal to fully superconducting phase boundary is at nonzero Josephson coupling in this regime, the early stages of the renormalization will affect the *location* of the critical manifold in the full parameter space. Thus duality cannot be used to locate the phase boundaries. Nevertheless, duality is still useful in this intermediate region.

The low-energy properties of the system will be given by the effective actions that *do* exhibit duality. Thus universal properties near the transitions at pairs of points in resistance space should be dual even when the location of the transitions as functions of the Josephson couplings are not. In particular, as we have seen in the explicit perturbative calculations of the critical behavior in the intermediate region in the regimes in which the critical fixed point is at either very strong or very weak coupling, the critical exponents, such as the RG eigenvalue λ, which controls deviations from criticality, will be universal functions of the resistances with values on 12-member sets of points being the same by the duality and the threefold permutation symmetry.

For the highly symmetric case $R_1=R_2=r=R$, the duality is simply

$$\tilde{R}=\frac{R_Q^2}{3R}, \tag{73}$$

so that there is a self-dual point at $R=1/\sqrt{3}$ at which we expect the eigenvalue λ to attain its maximum and the associated correlation time exponent that controls the scaling of the temperature at which crossover will occur from critical to noncritical to be minimum

More generally, the fact that the duality of Eqs. (68) involves the combination Y in a simple way enables us to immediately find a self-dual condition

$$Y=rR_1+rR_2+R_1R_2=R_Q^2. \tag{74}$$

When this condition is satisfied, the system will be on the self-dual surface. In the intermediate region, we thus expect the exponent λ to be maximal on this surface and decrease in both directions away from it. On this surface, it will presumably vary.

VII. DISCUSSION

A. Relation to experiments

We now consider the consequences of the results obtained in this paper for the two junction system shown in Fig. 2.

Existence of the SC* phase. One new prediction is the SC* phase that is superconducting for lead-to-lead transport but has localized Cooper pairs on the middle grain. A similar phase has been discussed previously in the context of one-dimensional Josephson junction arrays.[50–52]

To observe the difference between the SC* and the fully superconducting phase in the transport between the two leads (labeled by ϕ_1 and ϕ_2 in Fig. 16), one must consider the nonlinear behavior, as in both phases there is no interlead resistance at zero current. But the transition SC* to FSC will be characterized by a discontinuous jump in the *exponent* of the nonlinear current-voltage characteristics, reflecting a change in the nature of the quantum phase slips in the two phases. In the SC* phase the system behaves essentially as one junction, and current is carried by lead-to-lead Cooper-pair cotunneling processes that are shunted by the effective resistance R_1+R_2. At $T=0$, for small currents we thus expect

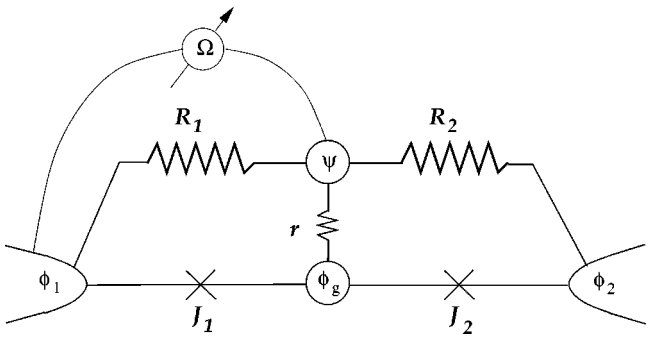

FIG. 16. Detection of the FSC to SC* phase transition. The transition between FSC and SC* will induce a jump in the effective resistance between the leads and grain. This can be observed by measuring the resistance between the lead 1 and the normal part of the grain. The resistance measured by Ω will increase from $(1/R_1+1/R_2+1/r)^{-1}$ in the FSC phase to $R_1R_2/(R_1+R_2)$ in the SC* phase. A similar discontinuity in the resistance will also occur at other phase boundaries; see the discussion in Sec. VII A.

$$V\propto I^{\alpha_1}, \tag{75}$$

where

$$\alpha_1=2[R_Q/(R_1+R_2)-1]. \tag{76}$$

This form will also obtain at low temperatures and fixed current as long as $k_BT<hI/e$. But at low currents for positive temperature we expect

$$V\propto T^{\alpha_1} \tag{77}$$

(see Ref. 43).

In the FSC phase both junctions are superconducting and quantum phase slips can appear in each of the junctions. The shunting resistances for QPS's in junctions 1 and 2 are $R_1+rR_2/(r+R_2)$ and $R_2+rR_1/(r+R_1)$, respectively, so we expect at $T=0$ and small currents

$$V\propto[\max(T,I/e)]^{\alpha_2}, \tag{78}$$

with

$$\alpha_2=2(R_Q/(R_{max}^{eff}-1) \tag{79}$$

in terms of

$$R_{max}^{eff}=\max(R_1+rR_2/(r+R_2),R_2+rR_1/(r+R_1)). \tag{80}$$

Another way to distinguish the FSC and SC* phases is to measure resistances directly between the leads and grain, as

shown in Fig. 16. The effective resistances between the grain and leads should jump at the transition between the FSC and SC* phases. In order to measure this jump, consider adding to the circuit an ohm meter Ω measuring the resistance between the (normal) grain and lead one. The transition between FSC and SC* will be characterized by the measured resistance increasing from $(1/R_1+1/R_2+1/r)^{-1}$ to $R_1R_2/(R_1+R_2)$ which is a large change if r is small. This occurs because in the SC* phase the superconductivity on the grain is effectively decoupled to that current cannot flow through r.

The ohm meter could also probe other phase transitions. For instance, in the NOR and N1-S2 phases, the measured resistance would be R_1, while in the S1-N2 phase, it would be $R_1r/(R_1+r)$.

*Observation of T**. Another result of our analysis is the existence of a new temperature scale T^* set by the grain level-spacing-like parameter δ. At high temperatures $T \gg T^*$, the Josephson junctions are effectively decoupled with the dissipation set by individual shunt resistances R_1 and R_2 [see discussion below Eq. (22)]. At temperatures below T^*, in contrast, we have a system of strongly coupled Josephson junctions with the dissipation determined by the whole circuit. For example, in the case $r>R_Q$, the effective dissipation is the total shunting resistance R_1+R_2. One possible way to observe the crossover at T^* is to choose parameters so that $r>R_Q$, $R_{1,2}<R_Q$ but $R_1+R_2>R_Q$. For $T>T^*$ dissipation is then strong enough to stabilize superconductivity on the individual junctions and we expect that the measured resistance of the system will decrease with decreasing temperature. But below T^* the dissipation is no longer sufficient to stabilize phase coherence between the leads as $(R_1+R_2)/R_Q>1$. At this point the phase slip fugacities become relevant, and we expect an upturn in the linear resistance as the temperature is lowered further. The basic reason for this is that at lower temperatures, the superconductivity is determined by longer length-scale fluctuations that involve less dissipation; the superconductivity is more vulnerable to these than the higher temperature more dissipative fluctuations.

Universal vs nonuniversal behavior of the resistance at the transition. An interesting feature of the zero-temperature phase diagram, which contrasts with that of a single junction, is the occurrence of some of the normal-to-superconductor transitions at nonuniversal values of the *total resistance*. Other transitions will occur at universal values of the appropriate resistance.

(i) In the mixed phase S1-N2, the linear resistance of the whole circuit is $R_2+rR_1/(r+R_1)$ [junction 1 is superconducting, and junction 2 is insulating; see Fig. 8(b)]. When this resistance becomes equal to the quantum of resistance R_Q there is a transition into the superconducting state FSC. That this transition occurs at a universal value of the total resistance is not surprising: it is due to the ordering of the ''last'' nonsuperconducting junction in the otherwise superconducting circuit.

(ii) In the fully normal phase, the system has resistance R_1+R_2. At the transition point into the superconducting SC* phase $R_1+R_2=R_Q$, so we again have a universal total resistance. This transition into the SC* phase is like a global or ''long-wavelength'' one: it involves superconducting fluctuations of the longest length scale available: lead-to-lead cotunneling of Cooper pairs.

(iii) At the direct transition from NOR to FSC, R_1+R_2 does *not* assume a universal value. For example, in the limit of small r the transition takes place when both resistances are close to R_Q (see Figs. 4 and 7), so the total resistance will be around $2R_Q$ at the transition. When $r\to 0$ the two junctions are decoupled even at zero temperatures [see Eq. (25)]. This limit is an example of a ''local'' superconductor-to-normal transition in which the *resistance per junction* is equal to R_Q at the transition point. This is the limit that has been extensively considered in the literature.[37,46]

Tuning the superconductor-to-normal transition by changing the Josephson couplings. We have shown that the superconductor-to-normal transition in a two-junction system may be tuned by changing the Josephson couplings J_1 or J_2 as well as by changing the shunting resistances $R_{1,2}$. The former may be easier to control in experiments as demonstrated recently in Refs. 12–15.

Nonuniversality of the critical exponents. In Sec. VI we showed that the transition between the fully superconducting and fully normal phases is controlled by a fixed point at intermediate values of the Josephson couplings. The critical exponents of this transition are nonuniversal and vary continuously as the three resistances in the system change. Nonuniversality of the critical exponents at superconductor-normal transitions in the presence of dissipation has also been discussed in Refs. 29,30, and 70.

Symmetries of the two-junction system. In Sec. VI we discussed the rich symmetries of the two-junction system. In addition to the usual weak–strong-coupling duality[43,67] it exhibits a permutation triality. Exchanging the three resistances R_1, R_2, and r leaves the action and phase diagram essentially unchanged. These symmetries provide a powerful tool for studying the two-junction system; one need only investigate one corner of the phase diagram to be able to construct it in its entirety. The boundaries of the region in which there is an intermediate coupling fixed point (see Fig. 15) can be found from the triality and weak-strong duality transformations.

B. Broader relevance and open questions

The results obtained in this paper should provide hints that may help understand other superconductor-to-normal transitions, such as in thin wires[20,21] and in films.[4,5] It is often conjectured that such transitions can be described in terms of models of resistively shunted Josephson junctions. For example, in wires one might perhaps think of segments of wire of length ξ_0 (i.e., the superconducting coherence length or phase slip core size) as individual grains. Then to estimate the crossover temperature analogous to our T^* one could take both R and r of the order of the normal-state resistance of a single segment. This would yield a superfluid-to-normal relaxation rate that is of the order of T_c. The crossover temperature T^* is related to the energy level separation parameter δ in such a segment of wire of length ξ_0. Using dirty

limit expressions $T_c = 1.8\hbar D/\xi_0^2$, $R = \xi_0/(e^2 N_0 DA)$, and $\delta = (N_0 A \xi_0)^{-1}$, in terms of D, the diffusion coefficient, N_0, the density of states per unit volume, and A, the wire's cross section, we find $T^* \approx T_c$. So at all temperatures one should consider the effects of interactions between the effective ''Josephson junctions'' that link the ''grains''; i.e., effects analogous to those discussed in this paper.

One possibility is that for wires much longer than ξ_0, the superconductor-to-normal transition will be determined not by the resistance per coherence length, but by the *total* normal-state resistance. Such behavior has been observed recently in experiments of Bezryadin and Lan[20] where wires as long as 15 times ξ_0 had a normal-to-superconductor transition when their total normal-state resistance was close to R_Q (see, however, Refs. 21 and 71–73]).

There is, however, another effect that must be considered in the long-wire regime. When normal metallic wires are long enough that their resistance is of order $\hbar/e^2 = 4R_Q$, localization effects start to be important at low temperatures, specifically below the temperature at which the inelastic mean free path of the normal electrons is of the order of the length over which the wire has resistance of order $4R_Q$. It is thus not clear that there is a regime in which the dissipative effects discussed here can affect the superconductivity without localization effects also becoming important. At least naively, however, sections of length ξ_0 cannot have resistance R_Q for $T < T_c$, and the inelastic scattering length is smaller than the coherence length near T_c. Thus there may well be temperature regimes in which these collective effects are important but localization effects not. This clearly requires substantial further thought. Alternate geometries, such as configurations with a metal layer underlying the superconducting wire, may be the best candidates for avoiding some of these complications.

In the previous subsection we discussed the possibility of a surprising phenomenon in the two-junction system: a minimum of the resistance at a crossover temperature T^* with an upturn at lower temperatures. Qualitatively similar behavior has already been observed in experiments on Josephson junction arrays and superconducting films. It is likely that the disorder plays an important role in such systems—especially in granular films such as InO.[4,5] Close to superconductor-to-normal transitions in disordered materials, the behavior may be dominated by weak links that involve connections via mesoscopic-size grains. As the temperature is lowered below the local T^*, the effective dissipation shunting these links will change in a manner analogous to that of the pair of junctions in series through a small grain discussed in this paper. This could potentially account for the observed saturation of the resistance at low temperatures in systems that would appear to be becoming superconducting on the basis of their behavior at higher temperatures. Understanding of such systems would benefit from generalizing the analysis of the two-junction system presented here to arrays of superconducting grains and Josephson junctions in both one and two dimensions.

An important issue that we have not addressed is the microscopic nature of the charge relaxation between normal and superconducting fluids that we have introduced phenomenologically. We have assumed that at low frequencies this is Ohmic even in the limit of zero temperature, but even if this is indeed the case, r should certainly depend on details of the experimental system. If, in fact, the relaxation is sub-Ohmic or super-Ohmic in the low-temperature limit, this will be roughly equivalent to the $r \to \infty$ of $r \to 0$ cases discussed here. However, taking into account charge quantization effects on the super-to-normal fluid relaxation and the role of quasiparticles and their nonconservation may lead to qualitatively new effects. One question that must be considered is whether there will be enough low-energy excitations on scales below T^* to give rise to the dissipative effects that are crucial for the logarithmic dependence of the effective action of quantum phase slips on temperature. We leave these issues for future research.

VIII. SUMMARY

In this paper we have analyzed Cooper-pair tunneling between two macroscopic leads via a mesoscopic superconducting grain in the presence of Ohmic dissipation. We treated this system in terms of a two-fluid description to the grain by effectively splitting it into normal and superconducting parts with capacitative and galvanic couplings between the Cooper pairs and normal electrons. A phenomenological Ohmic resistance r was introduced to describe the charge relaxation between the superconducting and normal parts of the grain. The corresponding microscopic Hamiltonian was used to derive the quantum action in terms of which the analysis was carried out. We showed that there is a new temperature scale T^* that separates two very different regimes. For macroscopic grains, $T^* = 0$, so that the system is always in the high-temperature regime in which the two junctions are decoupled. In contrast, for small grains at temperatures below T^* there is strong coupling between the junctions and the system can be described by a two-component sine-Gordon model. We analyzed this model in the limit of weak Josephson coupling and showed that it leads to a rich quantum phase diagram with two superconducting and three nonsuperconducting phases. The most surprising result is the appearance of a novel superconducting phase SC* that has localized Cooper pairs on the grain but phase coherence between the leads due to Cooper-pair cotunneling processes.

The limit of strong Josephson coupling was studied using a dual two-component sine-Gordon model. Simple circuit theory for the two-junction system enabled us to derive the phase diagram for both the weak- and strong-Josephson-coupling limits. In contrast to the single-junction case, we demonstrated that the strong- and weak-coupling analyses predict different locations of the transition between the fully superconducting and fully normal phases, implying the existence of an intermediate-coupling fixed point controlling this transition. We analyzed the renormalization group flows in this intermediate regime and found nonuniversal critical behavior with the exponents depending continuously on the resistances involved, The rich symmetries of the two-component sine-Gordon model include weak- to strong-coupling duality and permutation triality of the shunting re-

sistors $R_{1,2}$ and relaxation resistance r.

Experimental implications of our model, including the crossover temperature T^*, the identification of the novel superconducting phase SC*, and the lack of universality of the measured resistance at the superconductor-to-normal transition, were discussed briefly. Finally, we noted that our results may be useful for understanding some of the puzzling properties of superconductor to normal transitions in thin wires and films.

ACKNOWLEDGMENTS

We would like to thank A. Amir, A. Bezryadin, S. Chakravarty, M. Dykman, E. Fradkin, L. Glazman, B. Halperin, W. Hofstetter, Y. Imry, R. Kapon, S. Kivelson, N. Markovic, D. Podolsky, L. Pryadko, M. Tinkham, and G. Zarand for helpful discussions. This research was supported by the National Science Foundation via Grant Nos. DMR-0132874 (E.D.) and DMR-9976621 (G.R., Y.O., and D.S.F.), by Harvard's Materials Research Science and Engineering Center, by the Sloan Foundation (E.D.), and by the Israeli Science Foundation via Grant No. 160/01-1 (Y.O.).

APPENDIX A: MICROSCOPIC MODEL

1. Microscopic model for a two-fluid network

In this appendix we provide the derivation of several important results used in Sec. II B. For generality, the first part of our analysis is not restricted to the system shown in Fig. 2, but applies to any two-fluid network. The network consists of superconducting islands (which may be electrodes or grains). Each island i in this network is assumed to have part of its charge in the form of superconducting Cooper pairs, Q_{Si}, and part of the charge, Q_{Ni}, in the form of normal fluid. The Hamiltonian of the system consists of three pieces:

$$\mathcal{H}(Q_{Ni},Q_{Si},\phi_i,\psi_i)=\mathcal{H}_Q+\mathcal{H}_J+\mathcal{H}_{dis}. \tag{A1}$$

The charging part $\mathcal{H}_Q$ is given by Eq. (6), with κ_{ij} defined as in Eq. (5). The Josephson energy of the Cooper-pair tunneling between the grains is

$$\mathcal{H}_J=-\frac{1}{2}\sum_{ij} J_{ij}\cos(\phi_i-\phi_j). \tag{A2}$$

Dissipation between the islands, as well as charge relaxation between the Cooper pairs and normal fluid inside the islands, is described using the Caldeira-Leggett heat-bath model (see discussion in Secs. II A and II B) with resistances R_{ij} and r_i, respectively:

$$\mathcal{H}_{dis}=\frac{1}{2}\sum_{ij}\mathcal{H}_{bath}(R_{ij},2\psi_i-2\psi_j)+\sum_i \mathcal{H}_{bath}(r_i,\phi_i-2\psi_i). \tag{A3}$$

The commutation relations between charges and phases are given by Eq. (7). Note that the Heisenberg equations of motion on ϕ_i and ψ_i correctly reproduce Josephson relations as in Eqs. (8).

We use the Hamiltonian (A1) and the commutation relations (7) to construct the imaginary-time quantum action

$$Z=\int \mathcal{D}Q_{Ni}\mathcal{D}Q_{Si}\mathcal{D}\phi_i\mathcal{D}\psi_i\exp\left(2ie\sum_i\int_0^\beta d\tau Q_{Si}\dot{\phi}_i+ie\sum_i\int_0^\beta d\tau Q_{Ni}\dot{\psi}_i-\int_0^\beta d\tau\mathcal{H}(Q_{Ni},Q_{Si},\phi_i,\psi_i)\right). \tag{A4}$$

We remind the reader that in the presence of Ohmic dissipation the phase variables ϕ_i and ψ_i should be periodic at $\tau=0$ and $\tau=\beta$ (no phase twists by multiples of 2π are allowed).

After integrating out Q_{Ni} and Q_{Si} in Eq. (A4) we find

$$Z=\int \mathcal{D}\phi_i\mathcal{D}\psi_i\exp(-S_Q-S_J-S_{dis}),$$

$$S_Q=\int_0^\beta d\tau\left(\frac{1}{2(2e)^2}\sum_{ij}\dot{\phi}_iM_{Sij}\dot{\phi}_j+\frac{1}{2e^2}\sum_{ij}\dot{\psi}_iM_{Nij}\dot{\psi}_j+\frac{1}{(2e^2)}\sum_{ij}\dot{\phi}_iM_{SNij}\dot{\psi}_j\right),$$

$$S_J=-\frac{1}{2}\sum_{ij}\int_0^\beta d\tau J_{ij}\cos(\phi_i-\phi_j),$$

$$S_{dis}=\beta\sum_{\omega_n}\left(\frac{1}{2}\sum_{ij}\frac{R_Q|\omega_n|}{2\pi R_{ij}}|2\psi_{i,(\omega_n)}-2\psi_{j,(\omega_n)}|^2+\sum_i\frac{R_Q|\omega_n|}{2\pi r_i}|2\psi_{i,(\omega_n)}-\phi_{i,(\omega_n)}|^2\right), \tag{A5}$$

where the matrices M satisfy the equation

$$\begin{pmatrix}\hat{\kappa}_S^{-1} & \hat{C}^{-1}\\ \hat{C}^{-1} & \hat{\kappa}_N^{-1}\end{pmatrix}\begin{pmatrix}\hat{M}_S & \hat{M}_{SN}\\ \hat{M}_{SN}^T & \hat{M}_N\end{pmatrix}=\begin{pmatrix}\hat{1} & 0\\ 0 & \hat{1}\end{pmatrix}, \tag{A6}$$

where we defined [Eq. 5)]

$$\kappa_{Sij}^{-1}=C_{ij}^{-1}+D_{Si}\delta_{ij},$$
$$\kappa_{Nij}^{-1}=C_{ij}^{-1}+D_{Ni}\delta_{ij}. \tag{A7}$$

D_{Si} and D_{Ni} are the level spacings of the island i, and C_{ij} is the capacitance of the island network.

In mesoscopic grains, level spacings are already much smaller than the electrostatic capacitances, and this condition is even better satisfied in macroscopic electrodes. Hence, we can expand Eq. (A6) in $D_{S,N}$. It is useful to point out that this approximation does not require that every $D_{S,Ni}$ be smaller than any island of the C_{ij}^{-1} matrix, but only that $D_{S,Ni}$ be smaller than C_{ii}^{-1}. Hence, this expansion can be

applied even when we have a combination of macroscopic electrodes and mesoscopic grains. We obtain

$$M_{Sij}=\frac{\delta_{ij}}{D_{Si}+D_{Ni}}+s_i C_{ij} s_j,$$

$$M_{Nij}=\frac{\delta_{ij}}{D_{Si}+D_{Ni}}+\eta_i C_{ij}\eta_j,$$

$$M_{NSij}=-\frac{\delta_{ij}}{D_{Si}+D_{Ni}}+\eta_i C_{ij} s_j, \tag{A8}$$

where

$$s_i=\frac{D_{Ni}}{D_{Si}+D_{Ni}},$$

$$\eta_i=\frac{D_{Si}}{D_{Si}+D_{Ni}}. \tag{A9}$$

Therefore, we can use the following simple expression:

$$S_Q=\int_0^\beta d\tau\left(\frac{1}{2(2e)^2}\sum_i\frac{(\dot\phi_i-2\dot\psi_i)^2}{(D_{Si}+D_{Ni})}+\frac{1}{2(2e^2)}\sum_{ij}(s_i\dot\phi_i+\eta_i 2\dot\psi_i)C_{ij}(s_j\dot\phi_j+\eta_j 2\dot\psi_j)\right). \tag{A10}$$

The first term in Eq. (A10) tends to equilibrate the normal and superconducting fluids by introducing an energetic penalty for having different chemical potentials. For macroscopic grains level spacings are zero, so this term requires $\dot\phi=2\dot\psi$, which is the case considered in the literature previously. The second term in Eq. (A10) describes the usual Coulomb interaction between the islands, but the potential on each island is now give by the weighted average of the potentials of the two fluids:

$$\overline{V_i}=(s_i V_{Si}+\eta_i V_{Ni}). \tag{A11}$$

2. Equations of motion

As a consistency check on the quantum action (A5), it is useful to show that its equations of motion reproduce the familiar equations of electrodynamics. After taking functional derivatives of Eqs. (A5) with respect to ϕ_i and ψ_i and analytically continuing into real time, we have

$$\frac{1}{(2e)^2}\sum_j M_{Sij}\ddot\phi_j+\frac{1}{2e^2}\sum_j M_{SNij}\ddot\psi_j-\sum_j J_{ij}\sin(\phi_i-\phi_j)+\frac{r_i}{(2e)^2}(\dot\phi_i-2\dot\psi_i)=0,$$

$$\frac{1}{2e^2}\sum_j M^T_{SNij}\ddot\phi_j+\frac{1}{e^2}\sum_j M_{Nij}\ddot\psi_j-\sum_j\frac{1}{e^2R_{ij}}(\dot\psi_i-\dot\psi_i)+\frac{1}{(2e)^2 r_i}(\dot\phi_i-2\dot\psi_i)=0. \tag{A12}$$

From Eqs. (5), (8), and (A6) we have

$$Q_{Si}=\frac{1}{2e}\sum_j M_{Sij}\dot\phi_j+\frac{1}{e}\sum_j M_{SNij}\dot\psi_j,$$

$$Q_{Ni}=\frac{1}{e}\sum_j M^T_{SNij}\dot\phi_j+\frac{1}{e}\sum_j M_{Nij}\dot\psi_j. \tag{A13}$$

Equations (A12) may be written then as

$$\frac{dQ_{Si}}{dt}-\frac{1}{2e}\sum_j J_{ij}\sin(\phi_i-\phi_j)+\frac{V_{Si}-V_{Ni}}{r_i}=0,$$

$$\frac{dQ_{Ni}}{dt}+\sum_j\frac{V_{Ni}-V_{Nj}}{R_{ij}}-\frac{V_{Si}-V_{Ni}}{r_i}=0. \tag{A14}$$

These are the usual charge conservation equations: the Josephson form of the Cooper-pair tunneling current and Ohm's laws for the normal currents and the ''conversion currents'' between the Cooper pairs and the normal fluid.

3. Two leads Josephson coupled via a mesoscopic superconducting grain

We now apply our general discussion from Appendix A2 to the system shown in Fig. 1, a single mesoscopic grain between two superconducting electrodes. We assume that the electrodes are sufficiently large, so the superconducting and normal fluids are perfectly coupled in them, $\phi_1=2\psi_1$ and $\phi_2=2\psi_2$. From Eq. (A10) the charging part of our system can be written as

$$S_Q=\frac{1}{2(2e)^2}\int_0^\beta d\tau\sum_{ij}\dot\chi_i C^0_{ij}\dot\chi_j, \tag{A15}$$

where $\chi^T=(\phi_1,\phi_2,\phi_g,2\psi_g)$ and

$$\hat C^0=\begin{pmatrix} C_{11} & C_{12} & C_{1g}s_g & C_{1g}\eta_g \\ C_{12} & C_{22} & C_{2g}s_g & C_{2g}\eta_g \\ C_{1g}s_g & C_{2g}s_g & C_{gg}s_g^2+C_Q & C_{gg}s_g\eta_g-C_Q \\ C_{1g}\eta_g & C_{2g}\eta_g & C_{gg}s_g\eta_g-C_Q & C_{gg}\eta_g^2+C_Q \end{pmatrix}, \tag{A16}$$

where $C_Q^{-1}=D_{Sg}+D_{Ng}$, $s_g=D_{Ng}/(D_{Sg}+D_{Ng})$, and $\eta_g=D_{Sg}/(D_{Sg}+D_{Ng})$. It is convenient to change variables to the phase differences and the center-of-mass phase Φ, defined as

$$\Delta_1=\phi_g-\phi_1,$$

$$\Delta_2=\phi_2-\phi_g,$$

$$\Delta_g = \phi_g - 2\psi_g ,$$

$$\Phi = \frac{C_{11}+C_{12}+C_{1g}}{C_{tot}}\phi_1 + \frac{C_{22}+C_{12}+C_{2g}}{C_{tot}}\phi_2 + \frac{C_{1g}+C_{2g}+C_{gg}}{C_{tot}}s_g\phi_g + \frac{C_{1g}+C_{2g}+C_{gg}}{C_{tot}}\eta_g 2\psi_g , \tag{A17}$$

with $C_{tot}=C_{11}+2C_{12}+C_{22}+2C_{1g}+2C_{2g}+C_{gg}$. We have

$$S_Q = \frac{1}{2(2e)^2}\int_0^\beta d\tau \left(\sum_{\alpha\beta} \dot{\Delta}_\alpha \tilde{C}_{\alpha\beta}\dot{\Delta}_\beta + C_{tot}\dot{\Phi}^2 \right), \tag{A18}$$

where the indices α and β are summed over 1, 2, and g. It is useful to observe that the center-of-mass phase Φ is decoupled from the phase differences in Eq. (A18) and can be integrated out in the partition function.

We do not discuss the most general case of the capacitance matrix C_{ij}, but concentrate on the situation when the dominant capacitances are the mutual capacitances between electrode 1 and the grain, C_1, and electrode 2 and the grain, C_2. This corresponds to taking $C_{11}=C_1+\Delta C_1$, $C_{12}=0$, $C_{1g}=-C_1$, $C_{22}=C_2+\Delta C_2$, $C_{2g}=-C_2$, and $C_{gg}=C_1+C_2+\Delta C_g$. After some straightforward manipulations, we get

$$S_Q = \frac{1}{2(2e)^2}\int_0^\beta d\tau [C_1(-\dot{\Delta}_1+\eta_g\dot{\Delta}_g)^2 + C_2(\dot{\Delta}_2+\eta_g\dot{\Delta}_g)^2 + C_Q\dot{\Delta}_g^2 + C_{tot}\dot{\Phi}^2]. \tag{A19}$$

4. Circuit-theory approach to the two-fluid model

We can gain more intuition about the analysis presented in Sec. II A by considering effective circuits for the island network. As a first example, let us take a freestanding grain. The electrochemical potentials for the normal and superconducting electrons on the grain can be written in the form

$$V_{g,N} = \frac{Q_N+Q_{SC}}{C} + D_N Q_N ,$$

$$V_{g,SC} = \frac{Q_N+Q_{SC}}{C} + D_S Q_{SC} . \tag{A20}$$

Here C is the capacitance of the grain relative to the ground, and the D_i's are the inverses of the corresponding compressibilities. Equation (A20) describes the electrical system in Fig. 17. In addition to C, there are two more ''effective'' capacitors $1/D_{SC}$,$1/D_N$, which describe the extra potential drop produced by the level spacings in each part of the grain. As can be seen in Fig. 17, the charge on the capacitor C has to be equal to the total charge on the grain, Q_N+Q_{SC}.

The electrochemical potentials in Eqs. (A20) yield the charging part of the Hamiltonian:

$$\mathcal{H}_Q = \frac{1}{2C}(Q_N+Q_{SC})^2 + \frac{1}{2}D_N Q_N^2 + \frac{1}{2}D_S Q_{SC}^2 . \tag{A21}$$

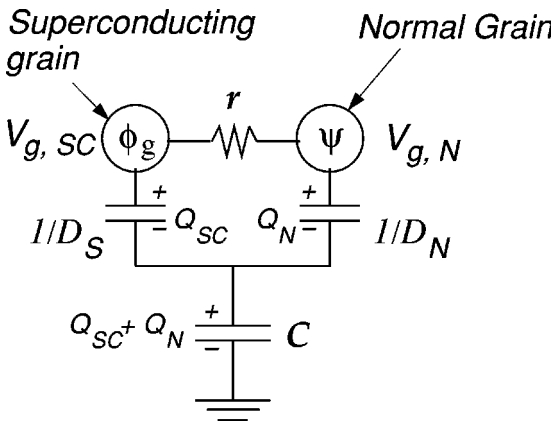

FIG. 17. The two-fluid model description of a freestanding, mesoscopic, superconducting grain. The grain is split into two grains: a superconducting-fluid grain, which contains Cooper pairs, and a normal-fluid grain, which contains the normal electrons. Normal electrons can become superconducting by flowing through r. The potential on the grains is given by a sum of the electrical potential, $(Q_N+Q_{SC})/C$, and a chemical contribution, $D_N Q_N$, and $D_S Q_{SC}$. The finite level spacings are modeled as capacitors with capacitances $1/D_N$,$1/D_S$.

From here on we could proceed along the lines of Appendix A1 to obtain the action for this circuit.

The general principal behind Eqs. (A20) is that the potential on each island consists of a sum of the electrical contribution, V_E, due to Coulomb interactions, and the level spacing contribution:

$$V_{g,N} = V_E + D_N Q_N ,$$

$$V_{g,SC} = V_E + D_{SC} Q_{SC} . \tag{A22}$$

If we construct a circuit for an island network, Eqs. (A22) indicate that we need to put the extra effective capacitors $1/D_{Ni}$, $1/D_{Si}$ between the point at which a macroscopic island would be and the normal and superconducting grains, respectively. Let us demonstrate this by constructing the effective circuit of the two-junction system.

The two-junction system consists of a mesoscopic superconducting grain situated between two macroscopic superconducting leads (Fig. 18). The capacitors C_1 and C_2 describe the ''bare'' interaction between the leads and grain. In addition to them, there are also the effective capacitors $1/D_N$ and $1/D_S$, which describe, respectively, the level spacing of the normal part and superconducting part of the mesoscopic grain (Fig. 18). These capacitors connect the point V_0, at which a macroscopic grain would have been, to the normal and superconducting parts of the mesoscopic grain.

The electrostatic part of the Hamiltonian of the two-junction system as shown in Fig. 18 is given by

$$\mathcal{H}_Q = \frac{1}{2C_1}Q_1^2 + \frac{1}{2C_2}Q_2^2 + \frac{1}{2}D_N Q_N^2 + \frac{1}{2}D_S Q_{SC}^2 , \tag{A23}$$

with the constraint

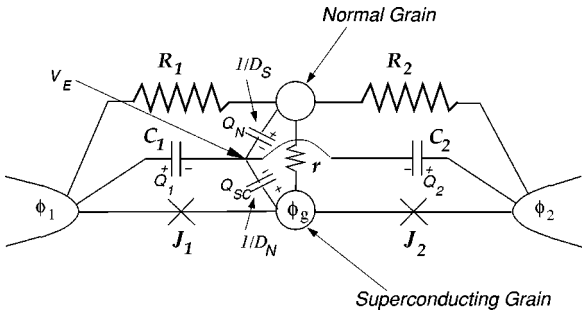

FIG. 18. The effective circuit of the two-Josephson-junction system. The mesoscopic grain is connected to the leads through Josephson junctions and resistors. It also interacts capacitatively with the leads. This interaction is modeled by the capacitors C_1, C_2 which connect to the two parts of the grain through additional capacitors $1/D_N, 1/D_S$. The additional capacitors account for the finite level spacings in the grain. The "bare" electrical potential on the grain (the electrochemical potential without the level-spacing contribution) is given by V_0, as noted in this figure.

$$Q_1+Q_2+Q_N+Q_{SC}=0. \tag{A24}$$

This constraint merely reflects the fact that the capacitors $1/D_{SC}$ and $1/D_N$ are not real capacitors, but an electrical analogy to the effects of the level spacings in the mesoscopic grain. The charge on the grain is $-Q_1-Q_2$ (where the minus sign is due to the convention in Fig. 18), and it is split into a superconducting part Q_{SC} and a normal part Q_N. In turn, Q_{SC} and Q_N increase the electrochemical potential on the grain, which is taken into account using the fictitious capacitors $1/D_{SC}, 1/D_N$.

We can use the constraint (A24) to eliminate the charge of the normal grain:

$$\mathcal{H}_Q=\frac{1}{2C_1}Q_1^2+\frac{1}{2C_2}Q_2^2+\frac{1}{2}\delta_N(Q_1+Q_2+Q_{SC})^2 + \frac{1}{2}\delta_{SC}Q_{SC}^2. \tag{A25}$$

One can now proceed by defining the phases ϕ_1, ϕ_2, and ϕ_g, which obey the commutation relations

$$[Q_1,\phi_1]=-2ie,$$
$$[Q_2,\phi_2]=-2ie,$$
$$[Q_{SC},\phi_g]=-2ie, \tag{A26}$$

and following steps presented in Appendix A1.

APPENDIX B: LOW-TEMPERATURE DISSIPATION

In the discussion in Sec. II we introduced the normal fluid of gapless quasiparticles as the origin of the dissipation for the junctions. This is not, however, a unique way of getting dissipation, including its Ohmic variety. From the various possibilities, let us mention exciting electromagnetic waves in the environment by fluctuations of the voltage and charge on the junctions. A well-studied example is a junction connected to an LC line [see Fig. 19(a)]. Sudden changes of the voltage in the junction excite plasmons, which carry the energy off to infinity (away from the junction), leading to dissipation. It can be described using effective impedance formalism[74]

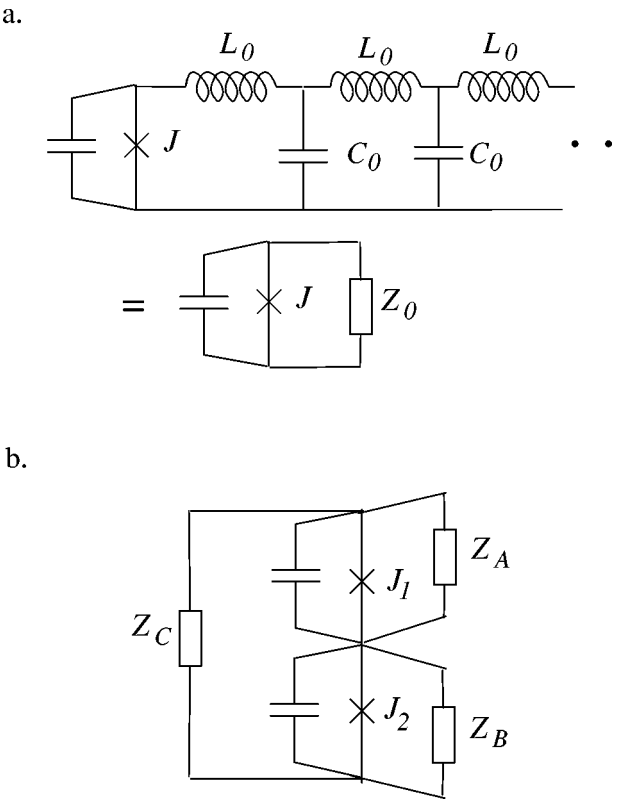

FIG. 19. An infinite transmission line as a source of dissipation. (a) A line of coils and capacitors L_0, C_0 has an effective real impedance $Z=\sqrt{L_0/C_0}$ at low frequencies. This line could describe electromagnetic modes that are excited by tunneling of Cooper pairs across junction J. (b) The two-junction system may have more than one transmission line. These lines are reduced in the figure to the effective impedances Z_A, Z_B, and Z_C. The schematic circuit shown has three effective shunt resistors, as in the model in Eq. (23). This configuration of effective impedances is the same as the "Δ" resistors network shown in Fig. 13. This will translate (using the Y-Δ transformation, Fig. 13) to the model in Eq. (23), with $R_1=Z_AZ_C/(Z_A+Z_B+Z_C)$, $R_2=Z_BZ_C/(Z_A+Z_B+Z_C)$, and $r=Z_AZ_B/(Z_A+Z_B+Z_C)$.

$$S_{dis}=\beta\sum_{\omega_n}\mathrm{Re}\left[\frac{R_Q}{Z[\omega]}\right]|\omega_n||\Delta\phi_{\omega_n}|^2, \tag{B1}$$

where $\Delta\phi$ is the phase difference across the junction and $Z(\omega)$ is the impedance of the environment seen by the junction. In the case of an infinite LC line $Z=(L_0/C_0)^{1/2}$, where L_0 and C_0 are inductance and capacitance per unit length, respectively, so we arrive at the Caldeira-Leggett-type Ohmic dissipation given in Eq. (14). For the system considered in this paper (see Fig. 1) such LC line (or its analogs) may come from the edges of the electrodes or the connecting wires. The crucial observation is that different Cooper-pair tunneling processes (between the two electrodes and the

grain, and the cotunneling process) should in general excite different electromagnetic waves. This can be seen from the schematic circuit shown in Fig. 19(b). The effective transmission lines in the figure give rise to three different resistors, which are related to R_1, R_2, and r from the model in Eq. (23), as discussed in the caption of Fig. 19. It is useful to point out that in this model we can relax the assumption of the small size of the grain, since the electromagnetic interactions discussed here, as well as the Josephson couplings, are present at all temperatures. In that case wires can be connected to each of the superconductors separately, allowing direct measurement of the rich phase diagram discussed in the bulk of the text, and effects related to charge discreteness are expected to be less significant. Dissipation due to other low-energy degrees of freedom in the system[75] is also possible.

It is worth emphasizing that the precise form of the quantum model for dissipation depends crucially on its nature. A common choice of the Caldeira-Legget Ohmic heat-bath model comes from the fact that it is the simplest quantum model consistent with the classical equations of motion. One expects that many effects of the dissipation would be at least qualitatively independent of its nature,[76] although considerable differences may also be present.

APPENDIX C: FREQUENCY SHELL RG

In order to find the phase diagram of a resistively shunted Josephson junction in the weak- or strong-coupling regime, it is best to employ a frequency shell RG. Generally we start with a sine-Gordon partition function such as

$$Z=\int D[\theta]\exp\left(-\int\frac{d\omega}{2\pi}\theta^2\frac{R|\omega|}{2\pi R_Q}+\int d\tau\frac{\zeta}{a}\cos(\theta)\right), \tag{C1}$$

where we have taken the $T\to 0$ limit and changed the ω sums into integrals. It is useful to redefine the amplitude of the anharmonic term using the short-time cutoff $a\sim 1/\omega_p$, where ω_p is the plasma frequency of the junction. The sharp high-frequency cutoff we use is

$$\Lambda\equiv\frac{\pi}{a}. \tag{C2}$$

As is well known,[77] the partition function (C1) is also the partition function of an interacting Coulomb gas in one dimension, with fugacity ζ and interaction

$$S_{ij(\tau)}=-2\sigma_i\sigma_j\frac{R_Q}{R}\ln\left|\frac{\tau}{a}\right|, \tag{C3}$$

where σ_i is the charge of the ith particle. In the weak-coupling limit (Sec. III A) the ''particles'' are pair-tunnel events and $\zeta=J$. In the strong-coupling limit Sec. IV the ''particles'' are quantum phase slips.

Presently we would like to integrate out the ''fast'' degrees of freedom associated with the field θ in Eq. (C1). This has the physical meaning of reducing the frequency cutoff Λ and can be thought of as *increasing* the effective size of a particle and eliminating all particle-antiparticle pairs whose separation is lower than this size. We write the action (C1) as

$$\begin{aligned}
Z=&\int D[\theta_<]\exp\left(-\int_{|\omega|<\Lambda-d\Lambda}\frac{d\omega}{2\pi}\theta^2\frac{R|\omega|}{2\pi R_Q}\right)\\
&\times\int D[\theta_>]\exp\left(-\int_{\Lambda-d\Lambda<|\omega|<\Lambda}\frac{d\omega}{2\pi}\theta^2\frac{R|\omega|}{2\pi R_Q}\right)\\
&\times\left(1+\frac{\zeta}{2a}\int d\tau(e^{i\theta_<}e^{i\theta_>}+e^{-i\theta_<}e^{-i\theta_>})+\cdots\right),\\
=&Z_<C\left(1+\int d\tau\frac{\zeta\exp\left(-\int_{\Lambda-d\Lambda}^{\Lambda}d\omega\frac{1}{R|\omega|}\right)}{2a}\right.\\
&\left.\times(e^{i\theta_<}+e^{-i\theta_<})+\cdots\right)\\
=&C\int D[\theta_<]\exp\left(-\int_{|\omega|<\Lambda-d\Lambda}\frac{d\omega}{2\pi}\theta^2\frac{R|\omega|}{2\pi R_Q}\right.\\
&\left.+\frac{\zeta\exp\left(-d\Lambda\frac{1}{R\Lambda}\right)}{a}\int d\tau\cos(\theta)\right).
\end{aligned} \tag{C4}$$

From this we obtain the RG flow

$$\frac{\zeta}{a}\to\frac{\zeta}{a}\left(1-\frac{R_Q}{R}\frac{d\Lambda}{\Lambda}\right). \tag{C5}$$

We still need to restore the variables to their original scale so that Eq. (C2) is fulfilled. Since $\Lambda\to\Lambda-d\Lambda$, $a\to a+da$. This leads to

$$\begin{aligned}
\frac{\zeta}{a}&\to\frac{\zeta}{a+da}\frac{a+da}{a}\left(1-\frac{R_Q}{R}\frac{d\Lambda}{\Lambda}\right)\\
&\to\frac{\zeta}{a+da}\left(1-\frac{R_Q}{R}\frac{d\Lambda}{\Lambda}+\frac{d\Lambda}{\Lambda}\right),
\end{aligned} \tag{C6}$$

which we can write as

$$\zeta\to\zeta\left(1-\frac{R_Q}{R}\frac{d\Lambda}{\Lambda}+\frac{d\Lambda}{\Lambda}\right)\frac{d\zeta}{dl}=-\Lambda\frac{d\zeta}{d\Lambda}=\zeta\left(1-\frac{R_Q}{R}\right), \tag{C7}$$

where the minus sign on the left-hand side of the middle equation denotes the fact that Λ is decreasing, and $dl\equiv -d\ln\Lambda$ with l the differential logarithmic flow scale parameter, $\Lambda=\Lambda_0 e^{-l}$.

From Eq. (C7) we see that when $R>R_Q$ ζ is relevant and the particles proliferate. When $R<1$ the opposite happens: all particles form dipoles that disappear when the scale increases.

APPENDIX D: COULOMB GAS REPRESENTATION OF THE WEAK-COUPLING LIMIT

In Appendix D2 we will derive the RG equations to second order of the two-component sine-Gordon model of Eq. (23). Before doing that, we will derive the Coulomb gas representation of this model (Appendix D1). This representation shows that the model (23) describes a gas of interacting pair-tunnel events. The Coulomb gas representation makes it conceptually easier to derive the second-order RG equations. In Appendix we use the Coulomb gas description to demonstrate how proliferated pair-tunnel events (or their strong-coupling counterparts, phase slips) screen other events. This adds to the discussion of the mixed phases in Secs. III B and IV B.

1. Coulomb gas representation

To analyze the two-junction system we use the mapping of the partition function (23) to a partition function of a Coulomb gas. The starting point for this investigation is the free energy that appears in Eq. (23):

$$S\approx\int\frac{d\omega}{2\pi}\frac{R_Q}{2\pi}\left(\Delta_1^2\frac{|\omega|\left(1+\frac{R_2}{r}\right)}{R_1+R_2+\frac{R_1R_2}{r}}+\Delta_2^2\frac{|\omega|\left(1+\frac{R_1}{r}\right)}{R_1+R_2+\frac{R_1R_2}{r}}+2\Delta_1\Delta_2\frac{|\omega|}{R_1+R_2+\frac{R_1R_2}{r}}\right)+\int\frac{d\tau}{a}[J_1\cos\Delta_1+J_2\cos\Delta_2+J_+\cos(\Delta_1+\Delta_2)],\tag{D1}$$

where we have redefined the anharmonic terms by a factor of $a\sim\omega_p^{-1}$.

The first step is to make use of the weak-coupling statement $J_{1,2}\ll 1$ and expand the exponent in a power law in the J's. Following that, an integration over the fields $\Delta_{1,2}$ reduces action (D1) to a partition function of an interacting gas with two kinds of charges, $\mu=1,2$, corresponding to $\exp(i\Delta_\mu)$:

$$Z=\sum_{n_1,n_2}\frac{J_1^{2n_1}}{(n_1!)^2}\frac{J_2^{2n_2}}{(n_2!)^2}\int\Pi_{i=1}^{2n_1}d\tau_i^{(1)}\Pi_{j=1}^{2n_2}d\tau_j^{(2)}\times\exp\left(-\frac{1}{2}\int d\tau_1 d\tau_2\sum_{\mu_1,\mu_2=1}^{2}\rho_{(\tau_1)}^{(\mu_1)}\rho_{(\tau_2)}^{(\mu_2)}S_{(\tau_1-\tau_2)}^{(\mu_1,\mu_2)}\right),\tag{D2}$$

where $\rho_{(\tau)}^{(\mu)}=\Sigma_{i=1}^{n_\mu}\sigma_i\delta_{(\tau-\tau_i)}$ is the density of the gas, and σ_i is the charge of the ith particle. J_1 and J_2 play the role of fugacities for the two types of gas particles.

The interaction actions are

$$S_{(\tau)}^{(11)}=-2\frac{(R_1+r)}{R_Q}\ln\left|\frac{\tau}{a}\right|,$$

$$S_{(\tau)}^{(22)}=-2\frac{(R_2+r)}{R_Q}\ln\left|\frac{\tau}{a}\right|,$$

$$S_{(\tau)}^{(12)}=2\frac{r}{R_Q}\ln\left|\frac{\tau}{a}\right|,\tag{D3}$$

where S^{ij} is the interaction energy between type-i particles and type-j particles. As we can see, the logarithmic divergent interactions impose the neutrality condition satisfied in Eq. (D2). Notice that gas particles of type 1 and type 2 of the same charge actually attract.

The meaning of each of the particles is very simple; a particle represents a *Cooper-pair tunneling* event through the corresponding junction (see Fig. 3).[43] To see this recall that, for example, $\Delta_1=\phi_g-\phi_1$ and the ϕ's are conjugate to the number of Cooper pairs on the corresponding grain or leads; hence the expansion in powers of J's leads to products of terms like $\exp[i(\phi_g-\phi_1)]$, which are translation operators for the charge difference between the middle grain and lead 1.

2. Two-component gas RG

To find the phase diagram of the two-junction system, we need to use both the mapping to a Coulomb gas from and the angular-frequency RG as described in Appendix C, extended to include second-order contributions. In order to make the discussion general, we will treat the following form of the action (23):

$$Z=\int\mathcal{D}\Delta_1\mathcal{D}\Delta_2 e^{-S_d-\tilde{S}_J},$$

$$\tilde{S}_J=\int_0^\beta\frac{d\tau}{a}[-J_1\cos(\Delta_1)-J_2\cos(\Delta_2)-J_+\cos(\Delta_1+\Delta_2)],$$

$$S_d=\int_{|\omega|<\Lambda}\frac{d\omega}{2\pi}|\omega|\vec{\Delta}_{(-\omega)}^T\hat{G}\vec{\Delta}_{(\omega)},\tag{D4}$$

with the capacitative part omitted, the sums over ω_n approximated by integrals, and the upper frequency cutoff $\Lambda=\pi/a$ introduced. The first-order contributions to the RG flow equations come from the terms linear in the J's and exactly following Appendix C, but using

$$\langle\Delta_i\Delta_j\rangle_\omega=\frac{1}{2\pi}\mathbf{G}_{ij}^{-1},\tag{D5}$$

we get the following first-order RG equations:

$$\frac{dJ_1}{dl}=J_1\left(1-\frac{1}{2\pi}\mathbf{G}_{11}^{-1}\right),$$

$$\frac{dJ_2}{dl}=J_2\left(1-\frac{1}{2\pi}\mathbf{G}_{22}^{-1}\right),$$

$$\frac{dJ_+}{dl}=J_+\left(1-\frac{1}{2\pi}(\mathbf{G}_{11}^{-1}+\mathbf{G}_{22}^{-1}+2\mathbf{G}_{12}^{-1})\right).\tag{D6}$$

The interactions between the two gas components give rise to second-order contributions to the RG equations. In addition, the second-order terms in the power-law expansion in J's of Eqs. (D4) produce corrections to the plasma frequency of the problem and other irrelevant operators.

First we will demonstrate how to derive all second-order contributions to the flow equations by deriving one such contribution. Let us consider an example for a second-order term. Then we will proceed to derive the unimportant plasma-frequency corrections.

Consider the term that results from the product of J_1 and J_2 first-order terms In a power-law expansion of Eqs. (D4),

$$Z=\cdots+\int D[\vec{\Delta}_<]D[\vec{\Delta}_>]\exp\left(-\int\frac{d\omega}{2\pi}\vec{\Delta}^\dagger\mathbf{G}\vec{\Delta}\right)\times\int d\tau_1\int d\tau_2\frac{J_1J_2}{4a^2}[e^{i(\Delta_{1(\tau_1)}+\Delta_{2(\tau_2)})}+e^{i(\Delta_{1(\tau_1)}-\Delta_{2(\tau_2)})}+\text{c.c.})]+\cdots. \tag{D7}$$

At this point we would like to integrate out the fast modes of the fields Δ_1,Δ_2 as in Eq. (C4). But we need to be careful since if $\tau_1=\tau_2$ the suppression resulting from the contraction of the fast modes is *not* the product of the two factors obtained from the first-order terms in J_1 and J_2:

$$\langle\cos(\Delta_1+\Delta_2)\rangle_{\Delta_1^>,\Delta_2^>}=\exp\left(-\frac{1}{2}\int_{\omega>\Lambda}\frac{d\omega}{2\pi}\langle(\Delta_1^>+\Delta_2^>)^2\rangle\right)\cos(\Delta_1+\Delta_2)$$

$$=\exp\left(-\frac{1}{2}\int_{\omega>\Lambda}\frac{d\omega}{2\pi}(\mathbf{G}_{11}^{-1}+\mathbf{G}_{22}^{-1}+2\mathbf{G}_{12}^{-1})\right)\times\cos(\Delta_1+\Delta_2). \tag{D8}$$

The renormalized second-order term, as in Eq. (D7), will only contain the self-interaction of a Cooper-pair tunneling event in junctions 1 and 2, completely dropping the $\exp(2\mathbf{G}_{12}^{-1})$. This difference produces a J_+ renormalization term. To calculate this term we first need to separate the contribution to the partition function that comes from the term (D7) to same time and different time contributions. Define $\tau=(\tau_1+\tau_2)/2, x=\tau_2-\tau_1$, and write

$$\int d\tau_1\int d\tau_2=\int d\tau\int dx=\int d\tau\int_{|x|>a+da}dx+\int d\tau\int_{|x|<a}dx+\int d\tau\int_{a<|x|<a+da}dx. \tag{D9}$$

The first integral is unaltered in the RG step (except for the influence on J_i of the integration of fast modes as in first order) and can be reexponentiated. The second term represents two gas particles of types 1 and 2 occurring at the same time, with the resolution of this RG step. This event too should be reexponentiated since it is also obtained as a second-order event in the renormalized variables. However, as pointed out in the previous paragraph, there is a discrepancy in the RG suppression coming from the fast mode contraction. Hence we write

$$\int\frac{d\tau}{a}\int_{|x|<a+da}\frac{dx}{a}\frac{J_1J_2}{4}\langle(e^{i(\Delta_{1(\tau+x/2)}+\Delta_{2(\tau-x/2)})}+e^{i(\Delta_{1(\tau+x/2)}-\Delta_{2(\tau-x/2)})}+\text{c.c.})\rangle_{\Delta_1^>,\Delta_2^>}\approx\int\frac{d\tau}{a}\frac{a+da}{a}J_1J_2$$

$$\times\exp\left(-\frac{1}{2}\int_{\omega>\Lambda}\frac{d\omega}{2\pi}(\mathbf{G}_{11}^{-1}+\mathbf{G}_{22}^{-1})\right)\left(\cos(\Delta_{1(\tau)}-\Delta_{2(\tau)}\left\{1+\left[\exp\left(-\frac{1}{2}\int_{\omega>\Lambda}\frac{d\omega}{2\pi}(-2)\mathbf{G}_{12}^{-1}\right)-1\right]\right\}\right.$$

$$\left.+\cos(\Delta_{1(\tau)}+\Delta_{2(\tau)})\left\{1+\left[\exp\left(-\frac{1}{2}\int_{\omega>\Lambda}\frac{d\omega}{2\pi}(2)\mathbf{G}_{12}^{-1}\right)-1\right]\right\}\right)$$

$$=\int\frac{d\tau}{a+da}\frac{J_1'J_2'}{2}\left[\left(1+\frac{2}{2\pi}\mathbf{G}_{12}^{-1}\frac{|d\Lambda|}{\Lambda}\right)\cos(\Delta_{1(\tau)}-\Delta_{2(\tau)})+\left(1-\frac{2}{2\pi}\mathbf{G}_{12}^{-1}\frac{|d\Lambda|}{\Lambda}\right)\cos(\Delta_{1(\tau)}+\Delta_{2(\tau)})\right]. \tag{D10}$$

The second term in each of the brackets multiplying the cos terms are the corrections that feed into $J_-\cos(\Delta_1-\Delta_2)$ and $J_+\cos(\Delta_1+\Delta_2)$.

Equation (D10) leads to an additional J_1J_2 in $dJ_{-,+}/dl$. The same could be done to second-order terms that are products of J_+ and $J_{1,2}$. For instance, in the case of J_+ the complete flow equation to second order would be

$$\frac{dJ_+}{dl}=J_+\left(1-\frac{1}{2\pi}(\mathbf{G}_{11}^{-1}+\mathbf{G}_{22}^{-1}+2\mathbf{G}_{12}^{-1})\right)+\frac{1}{2\pi}\mathbf{G}_{12}^{-1}J_1J_2. \tag{D11}$$

The same equation with the sign of $\mathbf{G}_{12}^{-1}$ reversed applies to J_-. Similarly, the flow equation for J_1 (J_2) would have a contribution proportional to J_2J_+ (J_1J_+) and J_2J_+ (J_1J_+).

The third term in Eq. (D9) leads to terms in the action proportional to ω^2 and hence are unimportant. To see this we will use two examples that exhaust all possibilities. As the first case, let us look at the term in the second-order expansion (D7) proportional to J_1^2:

$$Z=\cdots+\int D[\Delta]\exp\left(-\int\frac{d\omega}{2\pi}\vec{\Delta}^{\dagger}\mathbf{G}\vec{\Delta}\right)\times\int d\tau_1\int d\tau_2\frac{J_1^2}{8a^2}(e^{i(\Delta_{1(\tau_1)}+\Delta_{1(\tau_2)})}+e^{i(\Delta_{1(\tau_1)}-\Delta_{1(\tau_2)})}+\text{c.c.})+\cdots. \tag{D12}$$

We ignore the first term in the brackets as it implies a very costly configuration of two particles very close to each other and concentrate on the second:

$$\int D[\Delta]\exp\left(-\int\frac{d\omega}{2\pi}\vec{\Delta}^{\dagger}\mathbf{G}\vec{\Delta}\right)\times\int d\tau\int_{a<|x|<a+da}dx\frac{J_1^2}{8a^2}(e^{i(\Delta_{1(\tau+x/2)}-\Delta_{1(\tau-x/2)})}+\text{c.c.}). \tag{D13}$$

Now

$$\int_{a<|x|<a+da}(e^{i(\Delta_{1(\tau+x/2)}-\Delta_{1(\tau-x/2)})}+\text{c.c.})\approx 2(e^{i\dot{\Delta}_{1(\tau)}a}+e^{-i\dot{\Delta}_{1(\tau)}a})\approx 2(2-\dot{\Delta}_{1(\tau)}^2a^2), \tag{D14}$$

but this can be reexponentiated to give a correction piece for the action:

$$\Delta S=\int d\tau da\frac{J_1^2}{4}\dot{\Delta}_{1(\tau)}^2=\int\frac{d\omega}{2\pi}da\frac{J_1^2}{4}\omega^2\Delta_1^2, \tag{D15}$$

which is just a ω^2 contribution that renormalizes the plasma frequency of the model.

A more complicated case would be considering again the term that mixes the two components of the gas:

$$Z=\cdots+\int D[\Delta]\exp\left(-\int\frac{d\omega}{2\pi}\vec{\Delta}^{\dagger}\mathbf{G}\vec{\Delta}\right)\times\int d\tau\int_{a<|x|<a+da}dx\frac{J_1J_2}{4a^2}(e^{i(\Delta_{1(\tau+x/2)}+\Delta_{2(\tau-x/2)})}+e^{i(\Delta_{1(\tau+x/2)}-\Delta_{2(\tau-x/2)})}+\text{c.c.})+\cdots. \tag{D16}$$

Here we use the following derivation:

$$\begin{aligned}\int_{a<|x|<a+da}&(e^{i(\Delta_{1(\tau+x/2)}+\Delta_{2(\tau-x/2)})}+\text{c.c.})\\&\approx da[e^{i(\Delta_{1(\tau)}+\Delta_{2(\tau)})}(e^{i(\dot{\Delta}_{1,(\tau)}-\dot{\Delta}_{2,(\tau)})a}+e^{-i(\dot{\Delta}_{1,(\tau)}-\dot{\Delta}_{2,(\tau)})a})+\text{c.c.}]\\&\approx 2da\cos(\Delta_{1(\tau)}+\Delta_{2(\tau)})\left(2-\frac{a^2}{4}(\dot{\Delta}_{1,(\tau)}-\dot{\Delta}_{2,(\tau)})^2\right).\end{aligned} \tag{D17}$$

This results then in the introduction of a term

$$\Delta S=\int d\tau da\frac{J_1J_2}{2}\cos(\Delta_{1(\tau)}+\Delta_{2(\tau)})\frac{(\dot{\Delta}_{1,(\tau)}-\dot{\Delta}_{2,(\tau)})^2}{4}, \tag{D18}$$

once again, proportional to ω^2, and hence, unimportant. Similarly,

$$\begin{aligned}\int_{a<|x|<a+da}&(e^{i(\Delta_{1(\tau+x/2)}-\Delta_{2(\tau-x/2)})}+\text{c.c.})\\&\approx da[e^{i(\Delta_{1(\tau)}-\Delta_{2(\tau)})}(e^{i(\dot{\Delta}_{1,(\tau)}+\dot{\Delta}_{2,(\tau)})a}+e^{-i(\dot{\Delta}_{1,(\tau)}+\dot{\Delta}_{2,(\tau)})a})+\text{c.c.}]\\&\approx 2da\cos(\Delta_{1(\tau)}-\Delta_{2(\tau)})\left(2-\frac{a^2}{4}(\dot{\Delta}_{1,(\tau)}+\dot{\Delta}_{2,(\tau)})^2\right),\end{aligned} \tag{D19}$$

yielding

$$\Delta S=\int d\tau da\frac{J_1J_2}{2}\cos(\Delta_{1(\tau)}-\Delta_{2(\tau)})\frac{(\dot{\Delta}_{1,(\tau)}+\dot{\Delta}_{2,(\tau)})^2}{4}. \tag{D20}$$

This exhausts all second-order contributions to the RG flow equations.

3. Screening of pair tunneling events

When discussing the phase diagram obtained from the RG flow Eqs. (27) in Sec. III, we had to account to parts of the phase diagram in which one of the three Josephson couplings is relevant; then we used the procedure of setting the respective phase-difference variable to zero, which is equivalent to starting from a new fixed point. Here we review this step and show that in the language of the Coulomb gas analogy, this procedure may be understood as screening of charges of one type by proliferated charges of the other type.

Let us start by considering the case of J_2 being relevant. The simplest approach to the strong-coupling limit is to assume that $\Delta_2=0$. This can be done because if $J_2\gg 1$; then the term $J_2\cos\Delta_2$ in the action (23) constrains Δ_2 to be 0. The kinetic part of the action becomes

$$S_1 = \int \frac{d\omega}{2\pi}\frac{R_Q}{2\pi}\Delta_1^2 \frac{|\omega|\left(1+\frac{R_2}{r}\right)}{R_1+R_2+\frac{R_1R_2}{r}}, \tag{D21}$$

and hence the flow for J_1 (or J_+) would become

$$\frac{dJ_1}{dl} = J_1\left(1-\frac{R_1+R_2+\frac{R_1R_2}{r}}{R_Q\left(1+\frac{R_2}{r}\right)}\right), \tag{D22}$$

shifting the phase boundary S1-N2 and the FSC phase to

$$\frac{R_1+R_2+\frac{R_1R_2}{r}}{1+\frac{R_2}{r}} = R_Q. \tag{D23}$$

The above calculation is a very straightforward way of obtaining the phase diagram; however, to understand the physics behind it let us take a step back. When J_2 is relevant, pair-tunnel events in junction 2 will proliferate. This means that any field felt by the gas particles of type 2 (corresponding to the pair-tunnel events in junction 2) will be *screened* by type-2 particles attracted to the source of the field. So every type-1 gas particle will acquire a *screening cloud* of particles of type 2, so that no field from the original type-1 particle is felt in junction 2. To make this a quantitative statement, a type-1 gas particle with charge q_1 exerts the field

$$q_1 S^{(12)}_{(\tau)} = 2q_1\frac{r}{R_Q}\ln\left|\frac{\tau}{a}\right|$$

on the type-2 particles. Type-2 particles will then form a screening cloud of charge q_2 so that

$$q_1 S^{(12)}_{(\tau)} = 2q_1\frac{r}{R_Q}\ln\left|\frac{\tau}{a}\right| = -q_2 S^{(22)}_{(\tau)} = 2q_2\frac{(R_2+r)}{R_Q}\ln\left|\frac{\tau}{a}\right|,$$

which leads to

$$q_2 = q_1\frac{r}{R_2+r}.$$

Now, the field that a test charge of type-1 would feel is

$$\begin{aligned} q_1 S'^{(11)}_{(\tau)} &= q_2 S^{(12)}_{(\tau)} + q_1 S^{(11)}_{(\tau)} \\ &= -2q_1\frac{1}{R_Q}\left(R_1+r-r\frac{r}{R_2+r}\right)\ln\left|\frac{\tau}{a}\right| \\ &= -2q_1\frac{1}{R_Q}\left(\frac{R_1+R_2+\frac{R_1R_2}{r}}{1+\frac{R_2}{r}}\right)\ln\left|\frac{\tau}{a}\right|, \end{aligned} \tag{D24}$$

which we see gives exactly the same result as Eq. (D23). Indeed this way is more complicated; however, it could also be employed in more complicated setups, and it gives some insight as to what physically happens to the system. In this case, the charge tunneling from lead 1 to the grain partially relaxes through the superconducting junction 2. The physical interpretation of the above results is also discussed in Sec. III C.

Next, let us consider the case of relevant J_+. Here we need to set $\Delta_1 = -\Delta_2 \equiv \Delta$. This gives a free energy kinetic part

$$S_+ = \int \frac{d\omega}{2\pi}\frac{R_Q}{2\pi}\Delta^2 \frac{|\omega|\left(\frac{R_1}{r}+\frac{R_2}{r}\right)}{R_1+R_2+\frac{R_1R_2}{r}}, \tag{D25}$$

and hence the flow for J_1 (or J_2) would become

$$\frac{dJ_1}{dl} = J_1\left[1-\frac{1}{R_Q}\left(r+\frac{R_1R_2}{R_1+R_2}\right)\right]. \tag{D26}$$

This shifts the phase boundary between the SC* phase and FSC phase to

$$r+\frac{R_1R_2}{R_1+R_2} = R_Q. \tag{D27}$$

Here too, we can follow the screening principal to get the answer. The idea would be that a pair-tunnel event would acquire a pair-tunnel couple screening cloud so that other pair-tunnel couples will not feel any field.

This method along with the self-consistent harmonic approximation[77] can be used to obtain more insight about the behavior of the system.

APPENDIX E: COULOMB GAS OF THE PHASE-SLIP REPRESENTATION OF THE STRONG-COUPLING CASE

1. Villain transformation: Phase slips

To treat the strong-coupling limit $J_1, J_2 \gg 1$, we need to derive a description of the two-junction system in terms of phase slips: events in which the phase of one of a Josephson junction tunnels from one trough of the Josephson cosine potential into an adjacent trough. This event leads to a voltage drop across the junction (from $\hbar\dot{\phi}/2e = V$) and hence to dissipation. To derive this action, we make use of the Villain transformation.[52,69,78]

Starting with the action (23)

$$S\approx\int\frac{d\omega}{2\pi}\frac{R_Q}{2\pi}\left(\Delta_1^2\frac{|\omega|\left(1+\frac{R_2}{r}\right)}{R_1+R_2+\frac{R_1R_2}{r}}+\Delta_2^2\frac{|\omega|\left(1+\frac{R_1}{r}\right)}{R_1+R_2+\frac{R_1R_2}{r}}+2\Delta_1\Delta_2\frac{|\omega|}{R_1+R_2+\frac{R_1R_2}{r}}\right)+S_C+S_J, \tag{E1}$$

with

$$S_J=\int d\frac{\tau}{a}(-J\cos\Delta_1-J\cos\Delta_2). \tag{E2}$$

Here too we modified the sum over frequencies into an integral and introduced a high-frequency cutoff.

The assumption of strong J allows us to perform a Villain transformation

$$\exp\left(\int d\tau J[\cos(\Delta_i)-1]\right)\approx\sum_{\eta^i_{(\tau)}}\exp\left(-\int d\tau\frac{J}{2}(\Delta_i+2\pi\eta^i_{(\tau)})^2\right), \tag{E3}$$

where $\eta^i_{(\tau)}$ maps imaginary time to the integers, and the sum on the right-hand side is over all these functions. The function $\eta^i_{(\tau)}$ specifies in which trough of the potential $J_i\cos\Delta_i$ the ith junction is. The essence of the Villain transformation is that it completely eliminates the dynamics of intratrough motion and only considers the tunneling between troughs. The intratrough near-minimum motion is encoded into what will become the fugacity of a phase slip, ζ_i.

It is actually better to use the Fourier transform of the time derivative: $\mathrm{FT}(\dot{\eta}^i_{(\tau)})=-i\omega\eta^i_{(\omega)}\equiv\rho^i_{(\omega)}$. Incorporating this allows us then to write

$$\exp(-S_J)\approx\sum_{\rho^{1,2}_{(\tau)}}\exp\left[-\int\frac{d\omega}{2\pi}\frac{J}{2}\left(\left|\Delta_1+2\pi\frac{\rho^1_{(\omega)}}{-i\omega}\right|^2+\left|\Delta_2+2\pi\frac{\rho^2_{(\omega)}}{-i\omega}\right|^2\right)\right]. \tag{E4}$$

Expanding the square and putting it all in the action (23) gives

$$S\approx\int\frac{d\omega}{2\pi}\left[\Delta_1^2\left(\frac{J}{2}+\frac{|\omega|\left(1+\frac{R_2}{r}\right)}{R_1+R_2+\frac{R_1R_2}{r}}\right)+\Delta_2^2\left(\frac{J}{2}+\frac{|\omega|\left(1+\frac{R_1}{r}\right)}{R_1+R_2+\frac{R_1R_2}{r}}\right)+2\Delta_1\Delta_2\frac{|\omega|}{R_1+R_2+\frac{R_1R_2}{r}}+\Delta_1J\frac{2\pi\rho_1}{i\omega}+\frac{J(2\pi\rho_1)^2}{\omega^2}+\Delta_2J\frac{2\pi\rho_2}{i\omega}+\frac{J(2\pi\rho_2)^2}{\omega^2}\right]. \tag{E5}$$

Recalling $Z=\Sigma_{\rho^{1,2}_{(\tau)}}\int D[\Delta_1]D[\Delta_2]\exp(-S)$, we are ready to integrate out Δ_1,Δ_2 and get the partition function for the phase-slip gas. After doing this and taking the limit of large J we get the following partition function:

$$Z=\sum_{\rho^{1,2}_{(\tau)}}\exp\left(\frac{R_Q}{2\pi}\int\frac{d\omega}{2\pi}\left\{(2\pi\rho_1)^2\frac{1}{|\omega|}\frac{1+\frac{R_2}{r}}{R_1+R_2+\frac{R_1R_2}{r}}+(2\pi\rho_2)^2\frac{1}{|\omega|}\frac{1+\frac{R_1}{r}}{R_1+R_2+\frac{R_1R_2}{r}}+2(2\pi\rho_1)\times(2\pi\rho_2)\frac{1}{|\omega|}\frac{1}{R_1+R_2+\frac{R_1R_2}{r}}\right\}\right). \tag{E6}$$

This is a partition function for a gas that consists of two kinds of particles, with ρ_1,ρ_2 being the densities of the two gasses. When carrying out the ω integrals we get the interaction between the gas particles. They are ($S^{(ij)}$ is the interaction between two positive particles, one of species i and the other from species j)

$$S^{(11)}_{(\tau)}=-2\frac{1+\frac{R_2}{r}}{R_1+R_2+\frac{R_1R_2}{r}}\ln\left(\frac{|\tau|}{a}\right)=-2\frac{1}{R_1+\frac{R_2r}{R_2+r}}\ln\left(\frac{|\tau|}{a}\right),$$

$$S^{(22)}_{(\tau)} = -2\frac{1+\frac{R_1}{r}}{R_1+R_2+\frac{R_1R_2}{r}}\ln\left(\frac{|\tau|}{a}\right)$$

$$= -2\frac{1}{R_2+\frac{R_1 r}{R_1+r}}\ln\left(\frac{|\tau|}{a}\right),$$

$$S^{(12)}_{(\tau)} = -2\frac{1}{R_1+R_2+\frac{R_1R_2}{r}}\ln\left(\frac{|\tau|}{a}\right). \qquad \text{(E7)}$$

As in the weak-coupling limit, here too we derived a Coulomb gas description of the action (23). However, in the strong-coupling limit the gas particles are phase slips, which produce a voltage drop over the junction.

2. From the Coulomb gas to sine-Gordon

The interacting gas of phase slips described in Eq. (E1) can be encoded into a new sine-Gordon theory, conjugate to the original theory (23). It is given by

$$Z = \int D[\theta_1]\int D[\theta_2]\exp\Bigg(-\int\frac{d\omega}{2\pi}\frac{|\omega|}{2\pi R_Q}[(r+R_1)\theta_1^2 + (r+R_2)\theta_2^2 - 2r\theta_1\theta_2] + \int\frac{d\tau}{a}[\zeta_1\cos(\theta_1) + \zeta_2\cos(\theta_2) + \zeta_-\cos(\theta_1-\theta_2)]\Bigg)$$

$$= \int D[\theta_1]\int D[\theta_2]\exp\Bigg(-\int\frac{d\omega}{2\pi}\vec{\theta}^{\dagger}\mathbf{G}\vec{\theta} + \int\frac{d\tau}{a}[\zeta_1\cos(\theta_1)+\zeta_2\cos(\theta_2)]\Bigg), \qquad \text{(E8)}$$

where $\zeta_{1,2}$ play the role of fugacities of the phase slips on junctions 1 and 2. By expanding this sine-Gordon theory in the ζ's and following the steps of Appendix D1 we recover the Coulomb gas described in Eqs. (E7).

[1] A. Auerbach, *Interacting Electrons and Quantum Magnetism* (Springer Verlag, New York, 1994).
[2] S. Sachdev, *Quantum Phase Transitions* (Cambridge University Press, Cambridge, England, 1999).
[3] A. Goldman and N. Markovic, Phys. Today **51**, 39 (1998).
[4] R.B. Barber, Jr. and R. Dynes, Phys. Rev. B **48**, 10 618 (1993).
[5] A. Frydman, O. Naaman, and R. Dynes, cond-mat/0302061 (unpublished).
[6] V. Gantmakher, M. Golubkov, V. Dolgopolov, G. Tsydynzhapov, and A. Shashkin, Physica B **284**, 649 (2000).
[7] V.F. Gantmakher, JETP **82**, 951 (1996).
[8] A. Yazdani and A. Kapitulnik, Phys. Rev. Lett. **74**, 3037 (1995).
[9] D. Ephron, A. Yazdany, A. Kapitulnik, and M. Beasley, Phys. Rev. Lett. **76**, 1529 (1996).
[10] N. Mason and A. Kapitulnik, Phys. Rev. Lett. **82**, 5341 (1999).
[11] R. Fazio and H. van der Zant, Phys. Rep. **355**, 235 (2001).
[12] C. Chen, D. Delsing, and D.H.T. Claeson, Phys. Scr. **T42**, 182 (1992).
[13] E. Chow, P. Delsing, and D. Haviland, Phys. Rev. Lett. **81**, 204 (1998).
[14] D.H.E. Chow and P. Delsing, Phys. Rev. Lett. **81**, 204 (1998).
[15] D.H.K. Anderson and P. Agren, Low Temp. Phys. **118**, 733 (2000).
[16] A.J. Rimberg *et al.*, Phys. Rev. Lett. **78**, 2632 (1997).
[17] Y. Takahide, R. Yagi, A. Kanda, Y. Ootuka, and S. Kobayashi, Phys. Rev. Lett. **85**, 1974 (2000).
[18] P. Delsing, C. Chen, D. Haviland, D.H.T. Bergsten, and T. Claeston, cond-mat/9805121 (unpublished).
[19] M. Watanabe and D.B. Haviland, cond-mat/0301340 (unpublished).
[20] A. Bezryadin and M.T.C.N. Lau, Nature (London) **404**, 971 (2000).
[21] C. Lau, N. Markovic, M. Bockrath, A. Bezryadin, and M. Tinkham, Phys. Rev. Lett. **87**, 217003 (2001).
[22] M. Tinkham and C. Lau, Appl. Phys. Lett. **80**, 2946 (2002).
[23] N. Giordano and E. Schuler, Phys. Rev. Lett. **63**, 2417 (1989).
[24] N. Giordano and E. Schuler, Phys. Rev. Lett. **61**, 2137 (1988).
[25] N. Giordano and E. Schuler, Phys. Rev. B **41**, 6350 (1990).
[26] N. Giordano and E. Schuler, Physica B **203**, 460 (1994).
[27] P. Xiong, A. Herzog, and R. Dynes, Phys. Rev. Lett. **78**, 927 (1997).
[28] A. Kapitulnik, N. Mason, S.A. Kivelson, and S. Chakravarty, Phys. Rev. B **65**, 125322 (2001).
[29] K.-H. Wagenblast, A. van Otterlo, G. Schn, and G.T. Zimnyi, Phys. Rev. Lett. **79**, 2730 (1997).
[30] K. Voelker, cond-mat/9911473 (unpublished).
[31] A. Larkin, Ann. Phys. **8**, 785 (1999).
[32] D. Dalidovich and P. Phillips, Phys. Rev. Lett. **84**, 737 (2000).
[33] B. Spivak, A. Zyuzin, and M. Hruska, Phys. Rev. B **64**, 132502 (2001).
[34] A. Caldeira and A. Leggett, Phys. Rev. Lett. **46**, 211 (1981).
[35] A. Caldeira and A. Leggett, Ann. Phys. (N.Y.) **149**, 374 (1983).
[36] A. Leggett, S. Chakravarty, M.F.A.T. Dorsey, A. Garg, and W. Zwerger, Rev. Mod. Phys. **59**, 1 (1987).
[37] S. Chakravarty, Phys. Rev. Lett. **49**, 681 (1982).
[38] A. Schmid, Phys. Rev. Lett. **51**, 1506 (1983).
[39] S. Bulgadaev, JETP Lett. **39**, 315 (1984).
[40] S. Korshunov, Sov. Phys. JETP **66**, 872 (1987).
[41] E. Simanek, *Inhomogeneous Superconductivity* (Oxford University Press, New York, 1994).
[42] U. Weiss, *Quantum Dissipative Systems* (World Scientific, Singapore, 2001).
[43] G. Schön and A. Zaikin, Phys. Rep. **198**, 238 (1990).
[44] J. Penttilä, Ü. Parts, P. Hakonen, M. Paalanen, and E. Sonin, Phys. Rev. Lett. **82**, 1004 (1999).

[45] S. Panyukov and A. Zaikin, Phys. Lett. A **156**, 119 (1991).
[46] M. Fisher, Phys. Rev. B **36**, 1917 (1987).
[47] S. Chakravarty, G. Ingold, S. Kivelson, and A. Luther, Phys. Rev. Lett. **56**, 2303 (1986).
[48] S. Chakravarty, S. Kivelson, and G. Zimányi, Phys. Rev. B **37**, 3283 (1988).
[49] P. Bobbert, R. Fazio, and G. Scön, Phys. Rev. B **45**, 2294 (1992).
[50] S. Korshunov, Sov. Phys. JETP **68**, 609 (1989).
[51] S. Korshunov, Europhys. Lett. **9**, 107 (1989).
[52] P. Bobbert, R. Fazio, G. Scön, and G. Zimányi, Phys. Rev. B **41**, 4009 (1990).
[53] A.M. van den Brink, A. Odintsov, P. Bobbert, and G. Schön, Z. Phys. B: Condens. Matter **85**, 459 (1991).
[54] G. Schön and A. Zaikin, Phys. Rev. B **40**, 5231 (1989).
[55] V. Ambegaokar, U. Eckern, and G. Schön, Phys. Rev. Lett. **48**, 1745 (1982).
[56] C. Bruder, R. Fazio, and G. Schön, Physica B **203**, 240 (1994).
[57] W. Skocpol, M. Beasley, and M. Tinkham, J. Low Temp. Phys. **16**, 145 (1974).
[58] M. Tinkham, Rev. Mod. Phys. **46**, 587 (1974).
[59] B. Ivlev and N. Kopnin, Adv. Phys. **33**, 47 (1984).
[60] Y. Nakamura, C. Chen, and J. Tsai, Phys. Rev. Lett. **79**, 2328 (1997).
[61] Y. Nakamura, A. Koretkov, C. Chen, and J. Tsai, Phys. Rev. B **56**, 5116 (1997).
[62] A. Cottet, D. Vion, A. Aassime, P. Joyez, D. Esteve, and M. Devoret, Physica C **367**, 297 (2002).
[63] R.J. Schoelkopf, A.A. Clerk, S.M. Girvin, K.W. Lehnert, and M.H. Devort, cond-mat/0210247 (unpublished).
[64] P. Hadley, M.R. Beasley, and K. Wiesenfeld, Phys. Rev. B **38**, 8712 (1988).
[65] M. Büttiker, H. Thomas, and A. Pretre, Phys. Lett. A **364–369**, 364 (1993).
[66] K. Likharev and A. Zorin, J. Low Temp. Phys. **59**, 347 (1985).
[67] M. Fisher and W. Zwerger, Phys. Rev. B **32**, 6190 (1985).
[68] R. Shankar, Phys. Rev. Lett. **46**, 379 (1981).
[69] U. Weiss, H. Grabert, P. Hänggi, and P. Riseborough, Phys. Rev. B **35**, 9535 (1987).
[70] A. Vishwanath, J.E. Moore, and T. Senthil, cond-mat/0209109 (unpublished).
[71] Y. Oreg and E. Demler, in *Electronic Correlations: From meso-to nano-physics, Proceedings of the XXXVI Rencontres de Moriond*, edited by G. M. T. Martin and J. T. T. Van (EDP Sciences, 2001).
[72] Y. Oreg and E. Demler, cond-mat/0106645 (unpublished).
[73] Y. Oreg and A. Finkel'stein, Phys. Rev. Lett. **84**, 191 (1999).
[74] G.-L. Ingold and Y. V. Nazarov, in *Single Charge Tunneling*, edited by H. Grabert and M. H. Devoret (Plenum Press, New York, 1992), Vol. 6, p. 21.
[75] P. Mohanty, E. Jariwala, and R. Webb, Phys. Rev. Lett. **78**, 3366 (1997).
[76] A. Leggett, in *Proceedings of the NATO Advanced Study Institute on Percolation, Localization, and Superconductivity*, edited by A. Goldman and S. Wolf (Plenum Press, New York, 1994).
[77] P. Minnhagen, Rev. Mod. Phys. **59**, 1001 (1987).
[78] J. Villain, J. Phys. (Paris) **36**, 581 (1975).